

Heat transfer in production and decay regions of grid-generated turbulence

G. Melina^{*1}, P. J. K. Bruce¹, G. F. Hewitt², and J. C. Vassilicos¹

¹Department of Aeronautics, Imperial College London, London SW7 2AZ, UK

²Department of Chemical Engineering, Imperial College London, London SW7 2AZ, UK

Abstract

Heat transfer measurements around the centreline circumference of a cylinder in crossflow are performed in a wind tunnel. The cylinder is placed at several stations downstream of three turbulence-generating grids with different geometries and different blockage ratios σ_g : a regular grid (RG60) with $\sigma_g = 32\%$, a fractal-square grid (FSG17) with $\sigma_g = 25\%$ and a single-square grid (SSG) with $\sigma_g = 20\%$. Measurements are performed at 20 stations for 3 nominal Reynolds numbers (based on the diameter D of the cylinder) $Re_\infty = 11\,100, 24\,500, 37\,900$. Hot-wire measurements are performed along the centreline, without the cylinder in place, to characterise the flow downstream of the grids. The extent of the turbulence production region, where the turbulence intensity Tu increases with the streamwise distance x from the grid, is higher for SSG and more so for FSG17 than for RG60. The angular profiles of the Nusselt number Nu are measured in the production regions of these two grids and are compared to those obtained in the decay regions, where Tu decreases with x . This comparison is made at locations with approximately same Tu . It is found that, for SSG, $Nu/Re^{0.5}$ on the front of the cylinder (boundary layer region) is lower in the production region than in the decay region. This is explained by the presence of clear and intense vortex shedding in the production region of SSG which reduces the turbulent fluctuations which are “effective” in enhancing the heat transfer across a laminar boundary layer. For higher Re_∞ , the values of $Nu/Re^{0.5}$ on the front of the cylinder are higher in the production region of FSG17 than in that of SSG, despite Tu being higher for SSG. This is consistent with a lower intermittency of the flow for FSG17 caused by the presence of the fractal geometrical iterations. The recovery of Nu on the back of the cylinder (wake region) is appreciably higher in the production region than in the decay region for both FSG17 and for SSG. This can be due to the lower integral length scale ratio L_u/D in the production region and suggests, for the same Re_∞ , a reduction of the vortex formation length downstream of the cylinder, possibly promoted by the interaction between the wakes of the bars of the grid and the wake of the cylinder. At a large distance from the grids, the heat transfer enhancement is higher and it is more efficient for FSG17 and for SSG than for RG60. For high values of x in the turbulence decay region of the grids, the values of \overline{Nu} (circumferential average of Nu) are similar for FSG17 and for SSG and they are both appreciably higher than for RG60. This happens despite both FSG17 and SSG having a lower blockage ratio than RG60. The use of FSG17 has the practical advantage of combining high heat transfer rates on the cylinder with a weak vortex shedding from the grid.

Keywords: forced convection; circular cylinder; grid-generated turbulence

^{*}Email address for correspondence: g.melina13@imperial.ac.uk

Nomenclature

a_1	Strain rate parameter
C_ϵ	Dissipation coefficient, $C_\epsilon = \epsilon L_u / u'^3$
D	Diameter of the cylinder
E_{sh}	Energy of the vortex shedding from the largest bars of the grids
E_u	Power spectral density of u
f	Frequency
f_λ	“Effective” frequency
f_{sh}	Frequency of the vortex shedding from the largest bars of the grids
h	Heat transfer coefficient, $h = \frac{q_{conv}}{T_w - T_\infty}$
H	Height (width) of the wind tunnel’s working section (length of the cylinder)
I	Electric current
L_0	Distance between the largest bars of the grid
L_e	Dissipation length scale, $L_e = 1.5u'^3/\epsilon$
L_h	Length of the heated section of the cylinder
L_u	Integral length scale of u , $L_u = U\Theta_u$
Nu	Local Nusselt number, $Nu = \frac{hD}{\lambda_{film}}$
\overline{Nu}	Circumferentially averaged Nusselt number, $\overline{Nu} = \frac{1}{180} \int_0^{180} Nu(\theta) d\theta$
q_{cond}	Conductive heat flux
q_{conv}	Convective heat flux
q_{gen}	Input heat flux, $q_{gen} = V_h I / (\pi D L_h)$
q_{rad}	Radiative heat flux, $q_{rad} = \epsilon_h \sigma (T_w^4 - T_\infty^4)$
Re	Local Reynolds number, $Re = \frac{UD}{\nu_{film}}$
Re_∞	Inlet Reynolds number, $Re_\infty = \frac{U_\infty D}{\nu_\infty}$
t_0	Thickness of the largest bars of the grid in a plane parallel to the grid
t_h	Thickness of the heating foil
T	Temperature

- T_{film} Film temperature, $T_{film} = (T_w + T_\infty) / 2$
- Tp Turbulence parameter, $Tp = TuRe^{1/3}(L_u/D)^{-1/3}$
- Tu Turbulence intensity, $Tu = u'/U$
- Tu_{eff} "Effective" turbulence intensity, $Tu_{eff} = u'_{eff}/U$
- Tu_{peak} Maximum value of turbulence intensity on the centreline
- u Streamwise fluctuating velocity component
- u' RMS value of u
- u_{eff}^2 "Effective" turbulent kinetic energy
- U Local mean streamwise velocity
- U_∞ Inlet velocity
- V_h Voltage drop across the length of the heating foil
- x Streamwise distance from the grid
- x^* Wake-interaction length scale, $x^* = L_0^2/t_0$
- x_{peak} Centreline streamwise location of the maximum of turbulence intensity
- y Spanwise direction (origin of the reference system on the centre of the grid)

Greek symbols

- Δf Width of the frequency integration interval for the computation of E_{sh} and of u_{eff}^2
- δ Boundary layer thickness
- λ Thermal conductivity of air
- λ_h Thermal conductivity of the heating foil
- ν Kinematic viscosity of air
- σ Stefan-Boltzmann constant
- σ_c Blockage ratio of the cylinder
- σ_g Blockage ratio of the grid
- θ Angular position measured from the front stagnation point
- Θ_u Integral time scale of u
- ϵ Turbulent kinetic energy dissipation rate per unit mass
- ϵ_h Surface emissivity of the heating foil

Subscripts

∞ Inlet values (upstream of the grids)

film Evaluated at T_{film}

FSP Front stagnation point, $\theta = 0^\circ$

RSP Rear stagnation point, $\theta = 180^\circ$

w Wall values

1 Introduction

The effects of turbulent flows on the heat transfer from cylinders are of interest in different engineering applications. Several industrial devices use cylindrical geometries to exchange heat between a wall and a fluid in a turbulent regime. Examples of such devices are shell-and-tube heat exchangers, pressurised water reactors or water to air radiators (Hewitt, 2008) to name a few. Understanding how to increase the heat transfer by tuning the turbulence properties of the flow is highly desirable.

Different investigations have focused on the effects of some turbulent flow parameters on the heat transfer values for a cylinder in crossflow. Smith and Kuethe (1966) developed a theoretical model by assuming that in the proximity of the front stagnation point the Reynolds stresses are proportional to the turbulence intensity Tu in the free-stream (flow approaching the cylinder) and to the distance from the wall. Their model, supported by experimental results, showed that the Frossling number at the front stagnation point $Nu_{FSP}/Re^{0.5}$, which is invariant with Re for laminar free-stream conditions (Frössling, 1958), was directly proportional to the turbulence parameter $TuRe^{0.5}$, where Re is the Reynolds number based on the diameter D of the cylinder and on the mean streamwise velocity U . Kestin and Wood (1971) and Lowery and Vachon (1975) measured respectively the mass transfer and the heat transfer from a cylinder in a turbulent crossflow generated by grids in a wind tunnel. Both studies correlated the values of $Nu_{FSP}/Re^{0.5}$ with a second-degree polynomial function of $TuRe^{0.5}$. The properties of the turbulent flow approaching the cylinder affect the entire angular heat or mass transfer profile (Boulos and Pei, 1974; Sanitjai and Goldstein, 2001) and so the values of the angle-averaged Nusselt number \overline{Nu} . Similarly to Nu_{FSP} , \overline{Nu} was correlated with empirical fits as a function of both Re and Tu (e.g. Endoh et al., 1972; Sikmanovic et al., 1974; Lowery and Vachon,

1975; Mehendale et al., 1991; Kondjoyan and Daudin, 1995). The main conclusion from these investigations was that both Nu_{FSP} and \overline{Nu} are increased by larger values of Tu and that the enhancement is more evident at higher Re .

Several experiments have shown that the role of the integral length scale L_u of the incoming flow can also be important (Sak et al., 2007). Van Der Hegge Zijnen (1958) reported that for the same Re and Tu , \overline{Nu} increased with the ratio L_u/D for $0 < L_u/D < 1.6$ whereas it decreased for $L_u/D > 1.6$. Zukauskas et al. (1993) also found the presence of an optimal value of L_u/D for which \overline{Nu} is maximum, but in this case it occurred for $L_u/D = 10/Re^{0.5}$ in the range $10^4 < Re < 10^6$ and for $Tu = 0.5\%$. To predict the effect of L_u on the front stagnation point heat transfer, different relations have been developed in the form $Nu_{FSP}/Re^{0.5} \propto Tu^\alpha Re^\beta (L_u/D)^\gamma$ with $\alpha, \beta > 0$ and $\gamma < 0$ (see e.g. Ames and Moffat, 1990; Van Fossen et al., 1995; Ames, 1997; Sanitjai and Goldstein, 2001; Gandavarapu and Ames, 2013), thus showing that Nu_{FSP} is usually anti-correlated with L_u/D . On the contrary, the experimental results on the effect of L_u/D on the Nusselt number at the rear stagnation point, Nu_{RSP} , appear somewhat contradictory. Torii and Yang (1993) found that higher values of L_u/D caused a noticeable decrease of Nu_{RSP} while Yardi and Sukhatme (1978) and Sanitjai and Goldstein (2001) did not find an appreciable effect of the free-stream turbulence on the values of Nu_{RSP} .

The turbulent flow approaching the cylinder has been usually generated with perturbing grids placed upstream of the heat transfer model in a wind tunnel. Examples of these turbulence generators are regular square mesh grids, arrays of parallel wires, damping screens or perforated plates. Quintino (2012) measured \overline{Nu} for an electrically heated cylinder (made in copper) in crossflow which was mounted horizontally in a wind tunnel and placed at different distances from grids made of two vertical strips; \overline{Nu} was obtained from the electric power delivered to the cylinder and from the wall temperature which was uniform given the heating technique used in that experiment. Global heat transfer measurements were performed in the range $430 < Re_\infty < 1300$, where Re_∞ was the Reynolds number based on the diameter of the cylinder and on the bulk velocity of the flow obtained from the volumetric flow rate measured at the outlet of the wind tunnel. The results showed that \overline{Nu} had a maximum value for a certain distance from the grid and that it then monotonically decreased downstream of it. The author attributed this behaviour to an acceleration of the flow close to the grid (contraction effect) and to a subsequent reduction of what the author called “wake intensity”. The values of \overline{Nu} were found to increase with the blockage ratio σ_g of the grids. One might conclude that, in order to significantly enhance the

heat transfer, it is required to use turbulence generators with high σ_g , which produce also high pressure losses and therefore penalise the efficiency of the heat transfer augmentation. However in the experiment of Quintino (2012), velocity measurements were not conducted to characterize the flow downstream of the grids and local heat transfer measurements around the circumference of the cylinder were not performed either.

Wind tunnel experiments performed by Mazellier and Vassilicos (2010) showed that in the turbulence decay region, where Tu decreases with the downstream distance x from the grid, fractal square grids produce higher values of Tu than regular square-mesh grids with higher σ_g and similar effective mesh size M_{eff} . The use of these geometries allowed to also increase the streamwise extent of the turbulence production region, where Tu increases with x . The position x_{peak} where Tu is maximum, $Tu = Tu_{peak}$, on the centreline is proportional to the wake-interaction length scale $x^* = L_0^2/t_0$, where L_0 is the distance between the largest bars of the grid and t_0 is their thickness in a plane parallel to the grid. This is a geometric scaling parameter introduced by Mazellier and Vassilicos (2010) which is related to the location where the wakes originating from the largest bars (rectangular prisms) of the grid meet on the centreline. Gomes-Fernandes et al. (2012) demonstrated that both x_{peak} and Tu_{peak} are also functions of the free-stream turbulence intensity (upstream of the grid) and of the drag coefficient of the bars. Moreover they showed that the scaling $Tu_{peak} \propto t_0/L_0$ holds for the fractal square grids they tried. A fractal square grid insert was used by Cafiero et al. (2014) in a nozzle to enhance the heat transfer from a plate where the jet impinges normally. The results of this study showed that, for small nozzle-to-plate separations, the heat transfer on the plate was substantially higher when the fractal insert was used in place of a regular square grid insert with the same σ_g . Cafiero et al. (2015) attributed this result to a higher magnitude and persistence of streamwise vorticity produced by the fractal insert leading to more entrainment.

The results of the experiments on fractal-generated turbulence, and the scaling laws obtained, offer new possibilities for heat transfer augmentation on a circular cylinder in crossflow. In particular (i) the possibility to achieve high values of Tu for larger distances from the turbulence generator suggests that the heat transfer from a cylinder could also be enhanced over a broader streamwise extent. (ii) The opportunity of increasing Tu by designing a grid with a high t_0/L_0 and a low σ_g indicates the possibility to enhance the heat transfer more efficiently, i.e. with a lower static pressure drop across the grid. (iii) A larger extent of the turbulence production region downstream of the grid facilitates the placement of a cylinder in this region and measurement of

the heat transfer distribution there. The angular heat transfer profiles could then be compared to those measured in the decay region for the same turbulence generator and for the same turbulence intensity.

The present experimental investigation aims to explore these scenarios. A heated circular cylinder is placed vertically in a wind tunnel downstream of three turbulence-generating grids with different geometrical designs and different blockage ratios: a regular grid (RG60) with $\sigma_g = 32\%$, a fractal square grid (FSG17) with $\sigma_g = 25\%$ and a single square grid (SSG) with $\sigma_g = 20\%$. Preliminary hot-wire measurements, without the cylinder in place, are performed to characterise the flow downstream of the grids along the centreline. The angular heat transfer profiles in the median circumference of the cylinder are measured at several distances from each grid for three nominal Reynolds numbers, $Re_\infty = 11\,100, 24\,500, 37\,900$, with $Re_\infty = U_\infty D / \nu_\infty$, where U_∞ is free-stream velocity (upstream of the grids) and ν_∞ is the kinematic viscosity of air evaluated at the free-stream temperature T_∞ . The evolution of the average heat transfer coefficient for the different cases is quantified along the streamwise direction. For both FSG17 and SSG the heat transfer profiles are measured and compared in two positions, one in the production region and the other one in the decay region, where turbulence intensity is approximately the same. To the authors' knowledge no previous measurements of angular heat transfer profiles around a cylinder in the production region of grid-generated turbulence exist.

The remainder of this paper is structured as follows: in Section 2 the experimental set-up is described; in Section 3 the results of the experiment are presented and commented; finally Section 4 concludes the paper.

2 Experimental set-up

Velocity and heat transfer measurements are performed in an open-circuit wind tunnel. Its maximum velocity, when empty, is 33 m s^{-1} with a background turbulence intensity of about 0.1%. The working section is 3 m long and has a square cross section with height $H = 0.46\text{ m}$. The velocity U_∞ upstream of the grids is set by measuring the pressure difference across the contraction of the wind tunnel. The ambient pressure is measured with an absolute pressure gauge and the free-stream temperature T_∞ is measured with a K-type thermocouple.

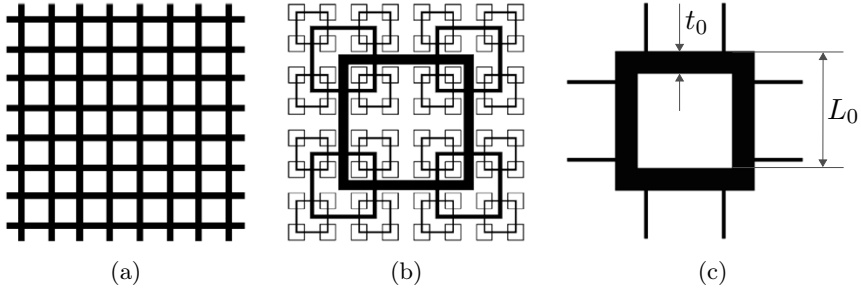


Fig. 1: Sketches of the turbulence-generating grids: RG60 (a), FSG17 (b), SSG (c).

Grid	σ_g [%]	L_0 [mm]	t_0 [mm]	x^* [mm]
RG60	32	60	10	360
FSG17	25	238	19	2950
SSG	20	229	43	1220

Tab. 1: Geometric parameters of the grids.

2.1 Grids

Three types of turbulence-generating grids are used in this experiment. Sketches of the grids are shown in Fig. 1 and their main geometric parameters are reported in Tab. 1. RG60 is a regular square-mesh bi-planar grid with the highest blockage σ_g and the smallest L_0 and t_0 . FSG17 is a multi-scale fractal square grid with four iterations, $N = 4$, and $t_r = t_0/t_{N-1} = 17$, where t_r is the thickness ratio and t_{N-1} is the thickness of the bars of the smallest fractal iteration. The ratio between the distance of the bars of two successive iterations is $R_L = L_{j+1}/L_j = 0.5$, the ratio between their thickness is $R_t = t_{j+1}/t_j = t_r^{1/(1-N)} = 0.39$ ($j = 0, 1, 2$). For a complete description of the fractal geometric parameters see Hurst and Vassilicos (2007). Finally SSG is a single square grid with the lowest σ_g and it is simply made of a single square and eight supporting struts. Note that SSG and FSG17 have a very similar L_0 but the ratio t_0/L_0 for SSG is more than double that for FSG17, $t_0/L_0 = 0.19$ for SSG and $t_0/L_0 = 0.08$ for FSG17.

One might argue that the comparison between the performance of the three selected grids is not fair as their blockage σ_g is not the same, $\sigma_g = 32\%$ for RG60, $\sigma_g = 25\%$ for FSG17, $\sigma_g = 20\%$ for SSG, and therefore they expectably produce a different pressure drop across the grid. This is indeed the case as shown by Melina et al. (2016) who measured the static pressure drop downstream of the same grids and found this is higher for RG60 than for both FSG17 and SSG. A goal of this experiment is to study if it is possible to enhance the heat transfer from the cylinder more efficiently, i.e. if the convective heat transfer can be increased more by using grids (FSG17 and SSG) with a blockage lower than for a reference regular grid (RG60). One can also notice

that the values of L_0 (mesh-size) and of x^* (wake-interaction length scale) are lower for RG60 than for both FSG17 and SSG. Previous research in grid-generated turbulence (see e.g. Valente and Vassilicos, 2014; Melina et al., 2016) has shown that flow characteristics such as homogeneity and large-scale isotropy, depend on the streamwise distance from the grid in terms of x/x^* . In particular one expects that, for $x > x_{peak}$, the higher x/x^* the higher the level of homogeneity and large-scale isotropy of the flow and the lower the turbulence intensity. A low value of x^* gives the chance to achieve high values of x/x^* (and so high levels of homogeneity) for a given length of the wind tunnel's test section. However, for a given distance from the grid, reducing x^* too much could cause the turbulence intensity to be too low to produce a significant effect on the heat transfer from the cylinder. The chosen values of x^* and L_0 for RG60 are chosen in order to: (i) measure the heat transfer from the cylinder in a condition of approximate homogeneous and isotropic turbulence to be compared with that measured downstream of FSG17 and SSG which have a higher x/x^* ; (ii) obtain a level of turbulence intensity which is high enough to produce an augmentation of the heat transfer at the selected positions for the cylinder; (iii) produce lower ratios L_u/D with respect to FSG17 and SSG (which have lower L_0 than RG60) so that the effect of the integral length scale L_u on the heat transfer enhancement could be investigated.

2.2 Velocity and heat transfer measurements

The flow downstream of each grid was first characterised without cylinder in place via single-component hot-wire measurements performed at a series of downstream positions x along the centreline. The sensing part of the wire was $5\ \mu\text{m}$ in diameter (d_w) and about 1 mm in length (l_w) so that the aspect ratio l_w/d_w was about 200. For each grid, velocity measurements were performed at $U_\infty = 5\ \text{m s}^{-1}$ and $U_\infty = 17\ \text{m s}^{-1}$, which correspond to the nominal Reynolds numbers $Re_\infty = 11\ 100$ and $Re_\infty = 37\ 900$ respectively. The cylinder was placed in the wind tunnel to perform the heat transfer measurements for the same range of U_∞ after the measurements for the grid turbulence without the cylinder were completed.

The sampling time for the hot wire measurements was 300s and corresponds to at least 29 000 – 97 000 integral time scales for the minimum and maximum Re_∞ respectively. The sampling frequency was set to be higher than twice the analogue low-pass filtering frequency, which was 30 kHz. The turbulence intensity is $Tu = u'/U$, where u' is the RMS value of the streamwise velocity fluctuations u , i.e. $u' = \sqrt{\langle u^2 \rangle} = \sqrt{\langle (\tilde{u} - U)^2 \rangle}$; \tilde{u} is the instantaneous velocity, U is the local mean velocity, $U = \langle \tilde{u} \rangle$, $\langle \cdot \rangle$ denotes the time-average operator.

The integral length scale was computed using Taylor’s hypothesis, $L_u = U\Theta_u$, where Θ_u is the integral time scale of u .

Once the turbulent flow downstream of the grids was characterised, a circular cylinder was mounted vertically in the wind tunnel and heat transfer measurements were performed around its median circumference for three nominal Reynolds numbers, $Re_\infty = 11\,100, 24\,500, 37\,900$. The diameter of the cylinder is $D = 35$ mm, its blockage is $\sigma_c = 7.6\%$ and its aspect ratio is $H/D = 13.1$. The cylinder comprises a central plastic tube, with length $L_h = 200$ mm, with top and bottom plastic sections. The central tube is delimited by two copper terminals and it is filled with Calcium-Magnesium Silicate insulating material. An Inconel foil with thickness $t_h = 25$ μm is wrapped and fixed around the central portion of the cylinder. The metallic foil is heated by Joule effect by delivering a direct electrical current I to the terminals using a laboratory power supply. This heating technique, similar to that used in Sanitjai and Goldstein (2004), approximates a uniform heat flux (UHF) on the cylinder’s wall.

A set of 8 K-type thermocouples is installed underneath the metallic foil to measure the wall temperature T_w . Fig. 2 is a sketch of the heated section of the cylinder and shows the location of the thermocouples. Thermocouples 1-4 are placed at 45° intervals and are used to measure the distribution of T_w around the circumference of the cylinder at its centre. This is accomplished by rotating the cylinder at 5° intervals using a stepper motor equipped with an optical encoder. The remaining thermocouples (5-8) can be used to check the uniformity of the wall temperature along the cylinder’s axis for a given angle. Preliminary measurements with a laminar free-stream were performed in order to validate the experimental technique at different Re_∞ (see Section 3.2). Note that in the case of laminar free-stream conditions the values of Re , based on the local U and on the kinematic viscosity ν_{film} evaluated at the film temperature $T_{film} = (T_\infty + T_w)/2$, and those of Re_∞ , based on U_∞ and on ν_∞ , are almost equivalent since U on the centreline coincides with U_∞ (ν_{film} is slightly higher than ν_∞). These measurements revealed that the difference between the wall temperature measured by thermocouples 5-8 and that measured by thermocouple 1 deviated by no more than 0.2% when these thermocouples were along the front stagnation line. This means that axial thermal conduction can be considered negligible for the cylinder used in the present experiment, at least in the proximity of the centreline circumference where the angular heat transfer profiles are measured.

The convective heat flux q_{conv} is obtained from the energy balance equation at the wall, $q_{conv} = q_{gen} - q_{rad} - q_{cond}$. The input heat flux q_{gen} is computed with $q_{gen} = V_h I / (\pi D L_h)$,

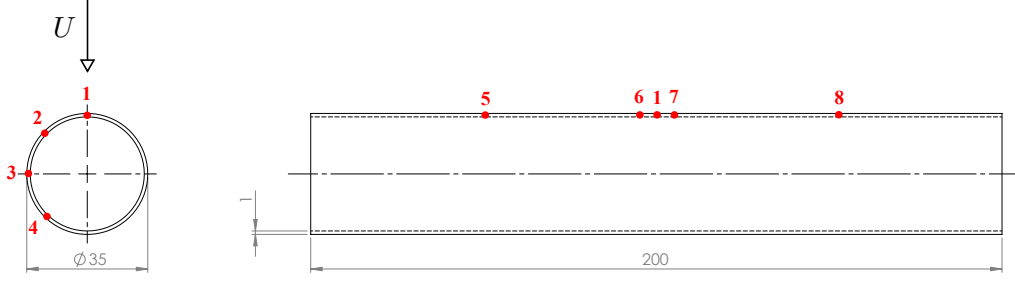


Fig. 2: Sketch of the heated section of the cylinder, dimensions in mm. The red dots identify the locations of the thermocouples (numbered 1 to 8).

where V_h is the measured voltage drop across the length of the heating foil (L_h). The term q_{rad} is the energy flux emitted by radiation and is estimated using the Stefan-Boltzmann law, $q_{rad} = \epsilon_h \sigma (T_w^4 - T_\infty^4)$ assuming $\epsilon_h = 0.1$ for the emissivity of the Inconel surface (Sanitjai and Goldstein, 2004). The term q_{cond} is the energy flux lost by thermal conduction which can be estimated with $q_{cond} = -\lambda_h t_h \nabla^2 T_w$ (Astarita et al., 2006), where λ_h is the thermal conductivity of Inconel. Since t_h is very small, the term q_{cond} is expected to be much smaller than q_{gen} . In the present configuration the most important contribution to the thermal conduction is expected to be the circumferential component since T_w varies in the angular direction (Lee and Kakade, 1976). The term q_{cond} can be therefore approximated as:

$$q_{cond} \approx -\lambda_h t_h \frac{4}{D^2} \frac{\partial^2 T_w}{\partial \theta^2}. \quad (1)$$

The ratio q_{cond}/q_{gen} is estimated to be maximum around $\theta = 90^\circ - 100^\circ$ for the minimum Re_∞ , the worst case scenario since the imposed q_{gen} is also minimum, whereas it is near-zero in the rest of the angular profile. In this worst case scenario the maximum value of q_{cond}/q_{gen} is about 5%. The value of \overline{Nu} (angle-average of Nu) changes always by less than 0.2% for all our measurements depending on whether the correction for thermal conduction is applied or not. Perkins and Leppert (1964) concluded that for their resistively-heated thin wall tube, the correction for thermal conduction in the circumferential direction was small and it applied just in one or two angular positions in their experiment (similarly to the case of the present experiment); it was therefore not taken into account for the computation of the local Nu around the cylinder. Given these figures, the correction for thermal conduction in the circumferential direction is not applied to the heat transfer results reported in this paper.

The local Nusselt number is calculated as $Nu = hD/\lambda_{film}$, where $h = q_{conv}/(T_w - T_\infty)$ is

Quantity	Typical value	Accuracy
D	35 mm	± 0.1 mm
L_h	200 mm	± 1 mm
V_h	2.1 V	$\pm 0.01 \times V_h$
I	23.2 A	$\pm 0.01 \times I$
T_∞	293 K	± 0.2 K
T_w	313 K	± 0.2 K
λ_{film}	$0.027 \text{ Wm}^{-1}\text{K}^{-1}$	$\pm 0.02 \times \lambda_{film}$
		Exp. uncertainty
h	$110 \text{ Wm}^{-2}\text{K}^{-1}$	$\pm 4.1\%$
Nu	142	$\pm 5.7\%$

Tab. 2: Typical values and associated measurement accuracies for the different quantities used to compute h and Nu , and typical relative experimental uncertainties (estimated using 95% confidence intervals) for the reported values of h and Nu .

the convective heat transfer coefficient and λ_{film} is the thermal conductivity of air evaluated at the film temperature T_{film} . Tab. 2 reports typical values and associated measurement accuracies for each quantity used to compute h and Nu . A single-sample uncertainty analysis using a 95% confidence interval is carried out following Moffat (1988). The typical resulting uncertainty errors on the computed values of h and Nu are 4.1% and 5.7% respectively.

3 Results and discussion

3.1 Flow downstream of the grids

Before placing the cylinder in the wind tunnel, the turbulent flow downstream of the grids is characterised with hot-wire measurements along the centreline, i.e. where the heat transfer measurements on the cylinder are also performed. Fig. 3a shows the evolution of the mean velocity normalised by U_∞ for the three turbulence generators. In all cases, the ratio U/U_∞ is initially high close to the grids and then decreases with x . For FSG17 this ratio is considerably higher than for RG60 and SSG in the near-grid field and it remains larger than 1 for a long downstream distance. This jet-like behaviour is believed to be caused by a strong acceleration of the flow due to the local small blockage near the center of FSG17 (Mazellier and Vassilicos, 2010). In other words the presence of the secondary geometrical iterations inside the biggest central square of FSG17 (see Fig. 1b) forces the flow to accelerate more at the center of the grid. This is different from SSG where there are no smaller iterations introducing blockage inside the big central square.

With regard to the turbulence intensity (Fig. 3b), RG60 produces the highest values of Tu

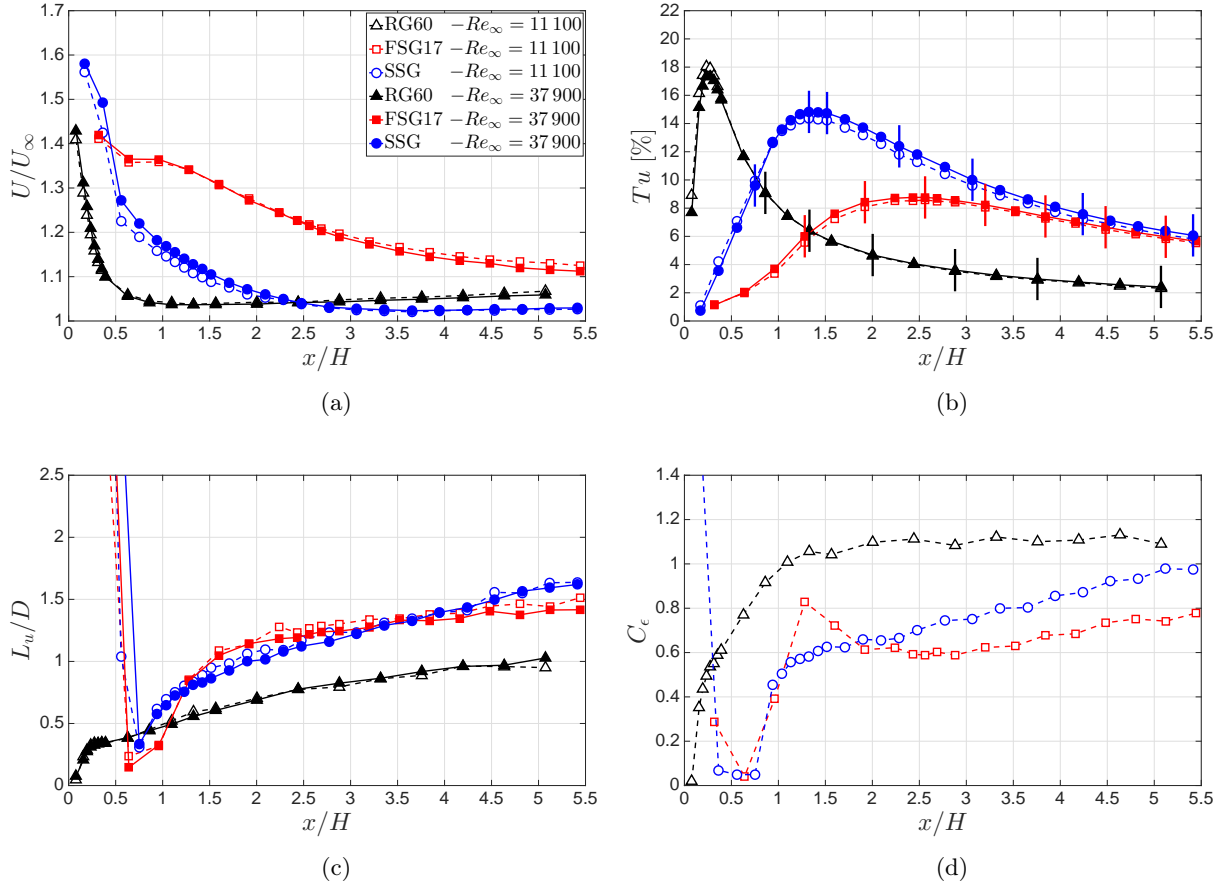


Fig. 3: Centreline mean velocity (a), turbulence intensity (b), integral length scale (c) and dissipation coefficient (d) for RG60, FSG17 and SSG. The vertical lines in (b) identify the positions where the heat transfer measurements on the cylinder are performed. Data in (d) are shown only for the measurements performed at $Re_\infty = 11\,100$ for which the spectrum of u is fully resolved.

very close to the grid, where Tu reaches approximately 18%. However it is clear that, when one moves downstream, the values of Tu rapidly decrease and become significantly lower than those of both FSG17 and SSG, despite RG60 having a higher σ_g . When compared with RG60, SSG and FSG17 produce a much extended turbulence production region, i.e. a higher x_{peak} . The value of x_{peak}/H (where Tu is maximum) is 0.24 for RG60, 1.33 for SSG and 2.56 for FSG17. The more extended production region for FSG17 and for SSG can be explained by the greater values of the wake interaction length scale x^* for these two grids than for RG60 (see Tab. 1). The grids SSG and FSG17 have a very similar L_0 but for SSG the value of t_0 is appreciably higher and therefore x^* is lower than for FSG17. This explains why x_{peak}/H is lower for SSG than for FSG17 and suggests that x^* is a more suitable parameter to scale x_{peak} than L_0 .

In Fig. 3b the vertical lines mark the 20 positions where the cylinder is placed to perform the heat transfer measurements. Note that the enlarged turbulence production regions for SSG

and FSG17 conveniently provide two positions for the cylinder, one in the production and the other in the decay, where Tu is approximately the same.

It is worth noting that Tu is larger for SSG than for FSG17, especially in the production region and in the proximity of x_{peak} . This happens despite SSG possessing a lower blockage σ_g than FSG17 and can be related to the fact that t_0/L_0 for SSG is more than twice that of FSG17 (see Gomes-Fernandes et al., 2012). As shown by Melina et al. (2016), the larger values of Tu for SSG than for FSG17 in the production region and even beyond x_{peak} can be explained by a much more energetic vortex shedding for SSG, i.e. for SSG the energy associated with the shedding frequency of its bars is higher than for FSG17 and so is its relative contribution to the magnitude of u'^2 at similar values of x/x_{peak} (see Section 3.3.1). One can see that the evolutions of Tu for SSG and FSG17 become very similar in the turbulence decay region for $x/H > 3.5$. This shows that the use of FSG17 facilitates the generation of a more extended turbulence production region, while still preserving high values of Tu in the decay region. Note that if both t_0 and L_0 (and so x^*) are kept the same, the values of Tu for a single square grid are substantially lower than those of a fractal square grid, as shown by Zhou et al. (2014).

The streamwise evolution of the integral length scale L_u is shown in Fig. 3c for the three grids. The values of L_u have been normalised with the cylinder's diameter D . The ratio L_u/D is lower for RG60 than for both FSG17 and SSG. This is a direct result of the significantly smaller value of L_0 for RG60 (see Tab. 1). For FSG17 and SSG, which have a very similar L_0 , the values of L_u/D are comparable. However for FSG17 the growth of L_u with x appears to be attenuated if compared to SSG. This effect could be a result of the reduced vortex shedding from the large bars of FSG17 with respect to SSG, as suggested by Melina et al. (2016).

One can see that both Tu (Fig. 3b) and L_u/D (Fig. 3c) do not significantly change with Re_∞ for the range investigated in this experiment. For this reason, it is the average values of Tu and of L_u/D over the measurements performed at both $Re_\infty = 11\,100$ and $Re_\infty = 37\,900$ which are considered when relating the heat transfer results to Tu and to L_u/D for the measurements taken at $Re_\infty = 24\,500$ in the following sections of the paper.

Fig. 3d shows the dissipation coefficient $C_\epsilon = \epsilon L_u/u'^3$ along the centerline, where the turbulent kinetic energy dissipation rate per unit mass ϵ is estimated assuming isotropy for the small scales and making use of Taylor's hypothesis, $\epsilon = 15 \nu_\infty \left\langle \left(\frac{\partial u}{\partial t} \right)^2 \right\rangle / U^2$. Only the measurements performed at the lowest Re_∞ are considered because in this case the frequency response of the hot-wire is high enough to fully resolve the energy spectrum of u . With the present

experiment we do not aim to understand if and how dissipation affects the heat transfer from the cylinder. However, presenting the data in Fig. 3d is useful to show that for FSG17 and SSG the velocity and the heat transfer measurements are performed in a region where $C_\epsilon \neq \text{constant}$. This is in contrast to the case with RG60, where C_ϵ reaches a constant value at about $x/H = 1.3$, which corresponds to approximately $x/x_{peak} = 5.5$. This distance (in terms of x/x_{peak}) is never reached in the present wind tunnel measurement for FSG17 and SSG as their wake interaction length scale x^* , and so x_{peak} , is considerably larger than for RG60. It is possible to speculate that proceeding farther downstream, i.e. reaching higher values of x/x_{peak} , we might expect C_ϵ to approach a constant value for FSG17 and SSG too (for a review on the topic see Vassilicos, 2015 and the more recent paper by Goto and Vassilicos, 2016).

3.2 Heat transfer under laminar free-stream conditions

Heat transfer measurements around the circumference of the cylinder are first performed under laminar free-stream conditions (without the grids in the wind tunnel) in order to validate the experimental technique and to have a baseline case. Measurements are performed at four Reynolds numbers, $10\,700 \leq Re \leq 41\,400$. It is useful to recall that, in the present case, Re and Re_∞ are almost equivalent given that U coincides with U_∞ , as mentioned in Section 2.2.

Fig. 4a shows the centreline angular profiles of Nu from the front stagnation point (FSP, $\theta = 0^\circ$) to the rear stagnation point (RSP, $\theta = 180^\circ$). Nu is observed to increase with Re with a maximum value at the FSP in each case. On the front of the cylinder ($\theta \lesssim 90^\circ$), Nu decreases with θ as a result of a growing boundary layer which is expected to be laminar in this region (Re is sub-critical) until separation occurs at $\theta = 85^\circ$ (Zdravkovich, 1997). In Fig. 4b the angular distributions of the Frossling number $Nu/Re^{0.5}$ are shown. The values of $Nu_{FSP}/Re^{0.5}$ are close to 1 within 1% among the four measurements, in good agreement with previous experimental results in air flows (see e.g. Eckert, 1942; Smith and Kuethe, 1966; Lowery and Vachon, 1975; Dullenkopf and Mayle, 1995; Kays et al., 2004) and so confirming that no significant heat conduction losses towards the inner core of the cylinder affect the measurements. In Fig. 4b (and in all other angular heat transfer profiles shown in this paper) the angular domain is divided in two regions: the first (labelled region A) refers to the front of the cylinder ($0^\circ < \theta < 85^\circ$), i.e. the boundary layer region; the second (labelled region B) refers to the back of the cylinder ($85^\circ < \theta < 180^\circ$), i.e. the wake region. A good collapse of the $Nu/Re^{0.5}$ profiles is obtained on the front of the cylinder (region A), thus confirming the presence of a laminar

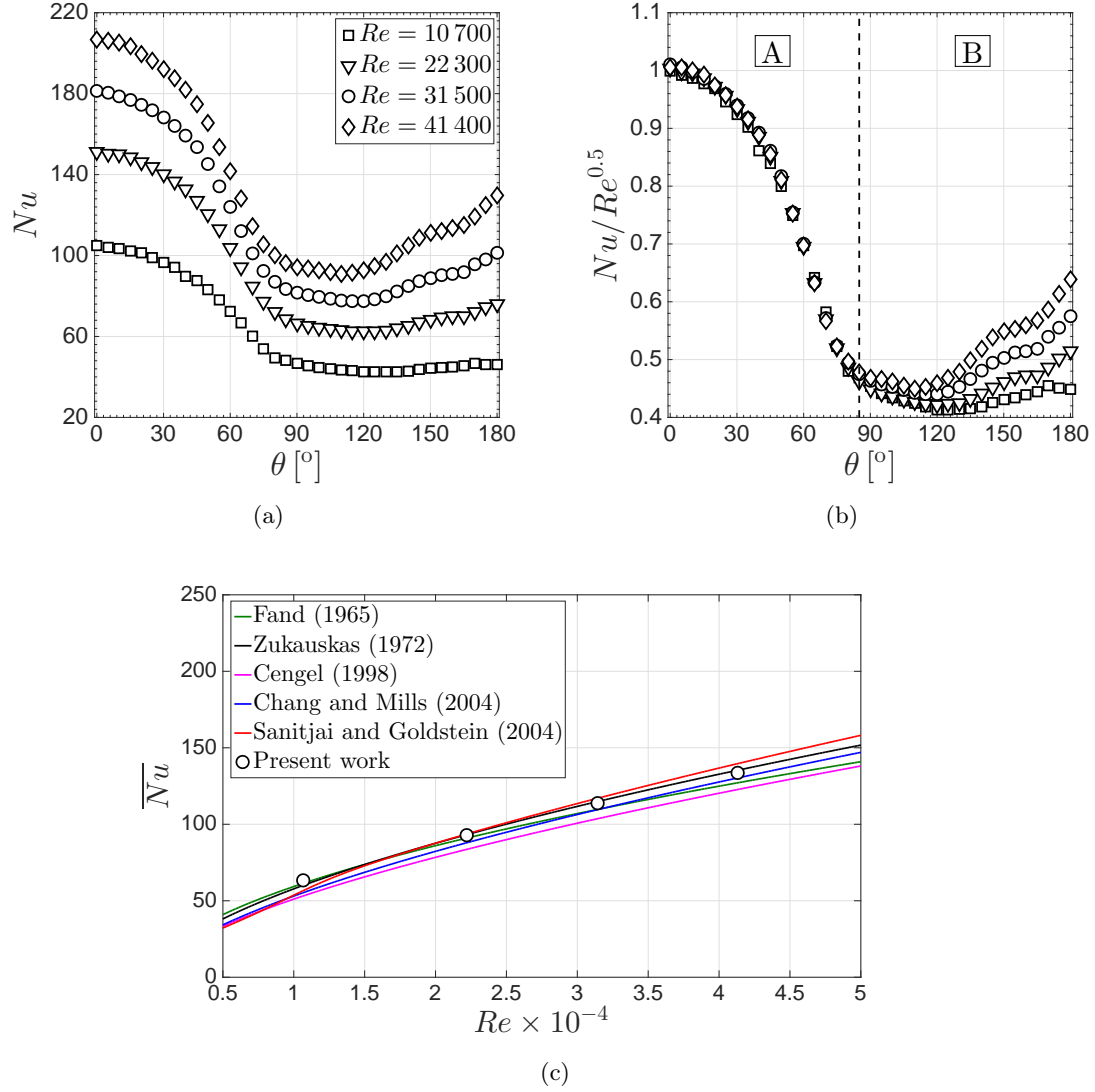


Fig. 4: Angular profiles of Nu (a) and of $Nu/Re^{0.5}$ (b), values of \overline{Nu} compared to those predicted by different empirical correlations as a function of Re (c). The vertical dashed line in (b) divides the angular domain in the boundary layer region (region A, $0^\circ < \theta < 85^\circ$) and in the wake region (region B, $85^\circ < \theta < 180^\circ$).

boundary layer there (Frössling, 1958).

On the rear of the cylinder (region B), where the flow is expected to be separated, the recovery of the heat transfer coefficient with respect to the FSP¹, Nu/Nu_{FSP} , consistently increases with Re (see Fig. 4b). This is particularly evident for $130^\circ < \theta < 180^\circ$, which is sometimes referred to as the “main vortex region” (Boulos and Pei, 1974). In this region, the greater values of Nu/Nu_{FSP} for increasing Re are explained by the fact that the vortex formation region moves closer to the cylinder as Re increases for $Re \gtrsim 1000$ (see e.g. Gerrard, 1978; Norberg, 1998; Lam

¹For the heat transfer results shown in Fig. 4, the angular profiles of Nu/Nu_{FSP} almost coincide with those of $Nu/Re^{0.5}$ since $Nu_{FSP}/Re^{0.5} \approx 1$ for laminar free-stream conditions.

et al., 2004), causing a stronger cooling effect from the turbulent periodic vortices shed from the cylinder as Re increases (Sanitjai and Goldstein, 2004).

For the highest Reynolds number, $Re = 41\,400$, the heat transfer recovery at the RSP is $Nu_{RSP}/Nu_{FSP} = 0.64$. Sanitjai and Goldstein (2004) obtained $Nu_{RSP}/Nu_{FSP} \approx 1$ for a comparable Reynolds number, $Re = 44\,800$. This higher value of Nu_{RSP}/Nu_{FSP} cannot be attributed solely to the slightly larger Re . Churchill and Bernstein (1977) warned that different experimental factors can affect the values of the heat transfer coefficient such as the heating condition, the blockage and the aspect ratio of the cylinder. In the present experiment the blockage and the aspect ratio of the cylinder are $\sigma_c = 7.6\%$ and $H/D = 13.1$ respectively. The results of Sanitjai and Goldstein (2004) were obtained for $\sigma_c = 14\%$ and $H/D = 4.2$. Chang and Mills (2004) investigated the effect of H/D on the heat transfer from a cylinder in crossflow. They found that when $H/D < 12$ the heat transfer coefficient on the rear of the cylinder decreased with increasing H/D and this effect was accentuated for increasing Re . For example they showed that for $Re = 33\,740$ the value of Nu_{RSP}/Nu_{FSP} decreased by about 32% when H/D increased from 6 to 12. These figures demonstrate that the lower value of Nu_{RSP}/Nu_{FSP} with respect to that obtained in Sanitjai and Goldstein (2004) is consistent with the higher aspect ratio of the cylinder used in the current experiment.

In Fig. 4c the circumferentially averaged values of the Nusselt number \overline{Nu} are compared to those predicted by different empirical correlations. A particularly good agreement is found with the correlation of Zukauskas (1972), $\overline{Nu} = 0.23Re^{0.6}$, from which the present results deviate by no more than 5%.

3.3 Heat transfer downstream of the grids

Heat transfer results for the cases with the cylinder placed downstream of the different grids are now presented and discussed.

In Fig. 5 the angular heat transfer profiles for RG60 are compared in two positions in the turbulence decay region, $x/H = 0.86$ and $x/H = 2.00$, where $Tu \approx 9.1\%$ and $Tu \approx 4.7\%$ respectively. Note that for these two positions the values of the local Re are very similar for the same Re_∞ since U/U_∞ is approximately the same (see Fig. 3a). The values of Tu and those of L_u/D taken as reference are the average values of those at the lowest and the highest Re_∞ presented in Fig. 3, measured on the centreline when the cylinder is not in place.

The values of $Nu/Re^{0.5}$ (Fig. 5a,b) on the front of the cylinder (region A) are higher than

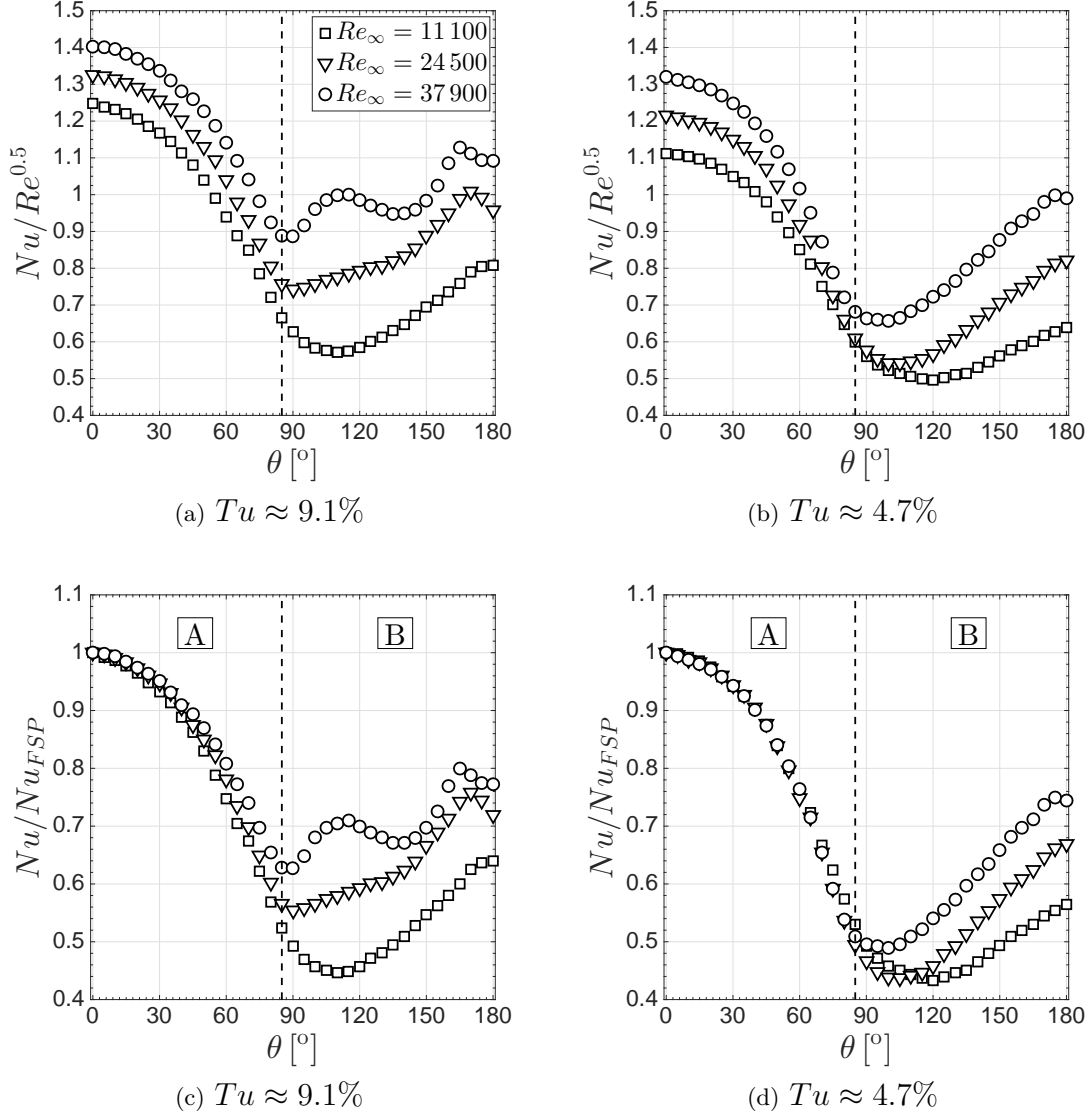


Fig. 5: Angular profiles of $Nu/Re^{0.5}$ (top) and of Nu/Nu_{FSP} (bottom) for RG60 in the decay region at $x/H = 0.86$ (left) and at $x/H = 2.00$ (right). The vertical dashed lines divide the angular domain in the boundary layer region (region A, $0^\circ < \theta < 85^\circ$) and in the wake region (region B, $85^\circ < \theta < 180^\circ$).

those for a laminar free-stream (Fig. 4b) and increase with Tu . The value of $Nu_{FSP}/Re^{0.5}$ is higher than 1 and increases with Re_∞ , thus showing that turbulence intensity is more effective in enhancing the heat transfer at higher Reynolds numbers. The profiles of Nu/Nu_{FSP} (Fig. 5c,d) almost collapse in region A (boundary layer region), more evidently in the proximity of the FSP and for the lower Tu .

In contradiction to the mass transfer results of Sanitjai and Goldstein (2001), the free-stream turbulence appears to affect the values of $Nu_{RSP}/Re^{0.5}$. In particular, here the values of $Nu_{RSP}/Re^{0.5}$ are higher with respect to the laminar free-stream case (see Fig. 4b) and are

observed to increase with Tu . An increasing trend of Nu_{RSP} with Tu at constant Re is shown for example in Boulos and Pei (1974) who obtained this result using a cylinder heated under UHF, as in the present investigation. It is worth mentioning that the mass transfer experiment of Sanitjai and Goldstein (2001) is different in that it approximates a uniform wall temperature (UWT) condition. Note that the decrease of $Nu_{RSP}/Re^{0.5}$ with x/H can be due to the combined effects of both the decrease of Tu and the increase of L_u/D (Torii and Yang, 1993) which, for RG60, is $L_u/D \approx 0.45$ at $x/H = 0.86$ and $L_u/D \approx 0.70$ at $x/H = 2.00$.

The turbulent flow approaching the cylinder affects the entire angular distribution over the rear face of the cylinder (region B). In particular when both Re_∞ and Tu are high enough (Fig. 5a,c), a characteristic ‘‘bump’’ appears in the separated part of the flow around $\theta = 115^\circ$. Sanitjai and Goldstein (2001) also found the presence of this bump at the same angular position. They argue that turbulent mixing associated with the reattachment of the flow is probably responsible for this feature. In Sanitjai and Goldstein (2001) the magnitude of this bump increases with Re and Tu , which is consistent with the plots in Fig 5. The presence of this localised increase in the heat transfer coefficient was also discussed by Achenbach (1975) who did experiments for a cylinder in crossflow with laminar free-stream conditions up to $Re = 4 \cdot 10^6$. This author showed, for example, that in the critical flow regime ($Re = 4 \cdot 10^5$) a significant increase in $Nu/Re^{0.5}$ occurs around $\theta = 120^\circ$, this being the location where he also measured an intensive rise in the skin friction coefficient, indicating the reattachment of the free shear layer on the cylinder’s wall.

3.3.1 Production and decay regions

As explained in Section 3.1, SSG and FSG17 produce an elongated turbulence production region. For these two grids it is therefore possible to place the cylinder in this region of the flow ($x < x_{peak}$) and to measure the resultant heat transfer profiles. These profiles can be compared to those measured in the decay region ($x > x_{peak}$), at points where Tu is approximately the same. This type of comparison is shown in Fig. 6 for SSG and in Fig. 7 for FSG17. The locations in the production region, $x/H = 0.75$ for SSG and $x/H = 1.28$ for FSG17, are chosen in order to have a similar x/x_{peak} for the two grids, $x/x_{peak} = 0.56$ for SSG and $x/x_{peak} = 0.50$ for FSG17. For both grids the values of Tu are very similar between the locations in the production region and those in the decay region, $Tu \approx 9.8\%$ for SSG and $Tu \approx 5.8\%$ for FSG17.

Comparison of Fig. 6a and Fig. 6b shows that for SSG the values of $Nu/Re^{0.5}$ on the front face of the cylinder (region A) are noticeably lower in the production region with respect to

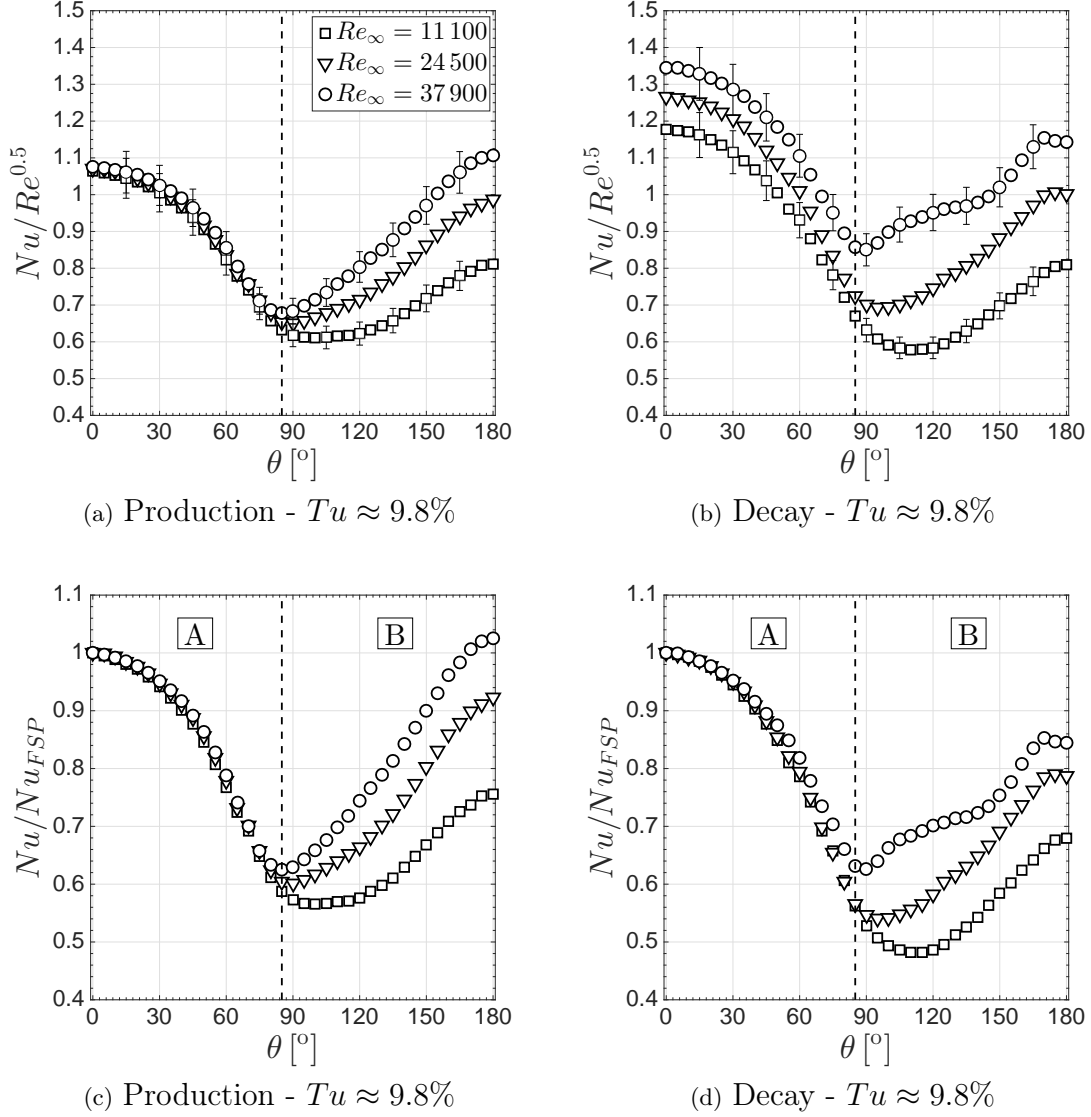


Fig. 6: Angular profiles of $Nu/Re^{0.5}$ (top) and of Nu/Nu_{FSP} (bottom) for SSG in the production region at $x/H = 0.75$ (left) and in the decay region at $x/H = 3.07$ (right). The vertical dashed lines divide the angular domain in the boundary layer region (region A, $0^\circ < \theta < 85^\circ$) and in the wake region (region B, $85^\circ < \theta < 180^\circ$). The error bars in (a) and (b) indicate the experimental errors evaluated via a single-sample uncertainty analysis with 95% confidence intervals.

the decay region, and more so for higher Re_∞ . On the front of the cylinder, the profiles of $Nu/Re^{0.5}$ in the production region of SSG are remarkably well collapsed in a similar manner to those obtained with laminar free-stream conditions (see Fig. 4b) despite Tu being quite high ($Tu \approx 9.8\%$). The value of $Nu_{FSP}/Re^{0.5}$ in the production region is only about 7% higher than that for a laminar free-stream, in contrast to the decay region where the enhancement reaches almost 35% for the highest Re_∞ . This result seems at first counter-intuitive for three reasons: (i) the value of Tu is approximately the same in the two regions, (ii) the local Re is higher in the production region given the greater values of U/U_∞ (see Fig. 3a), (iii) L_u/D is

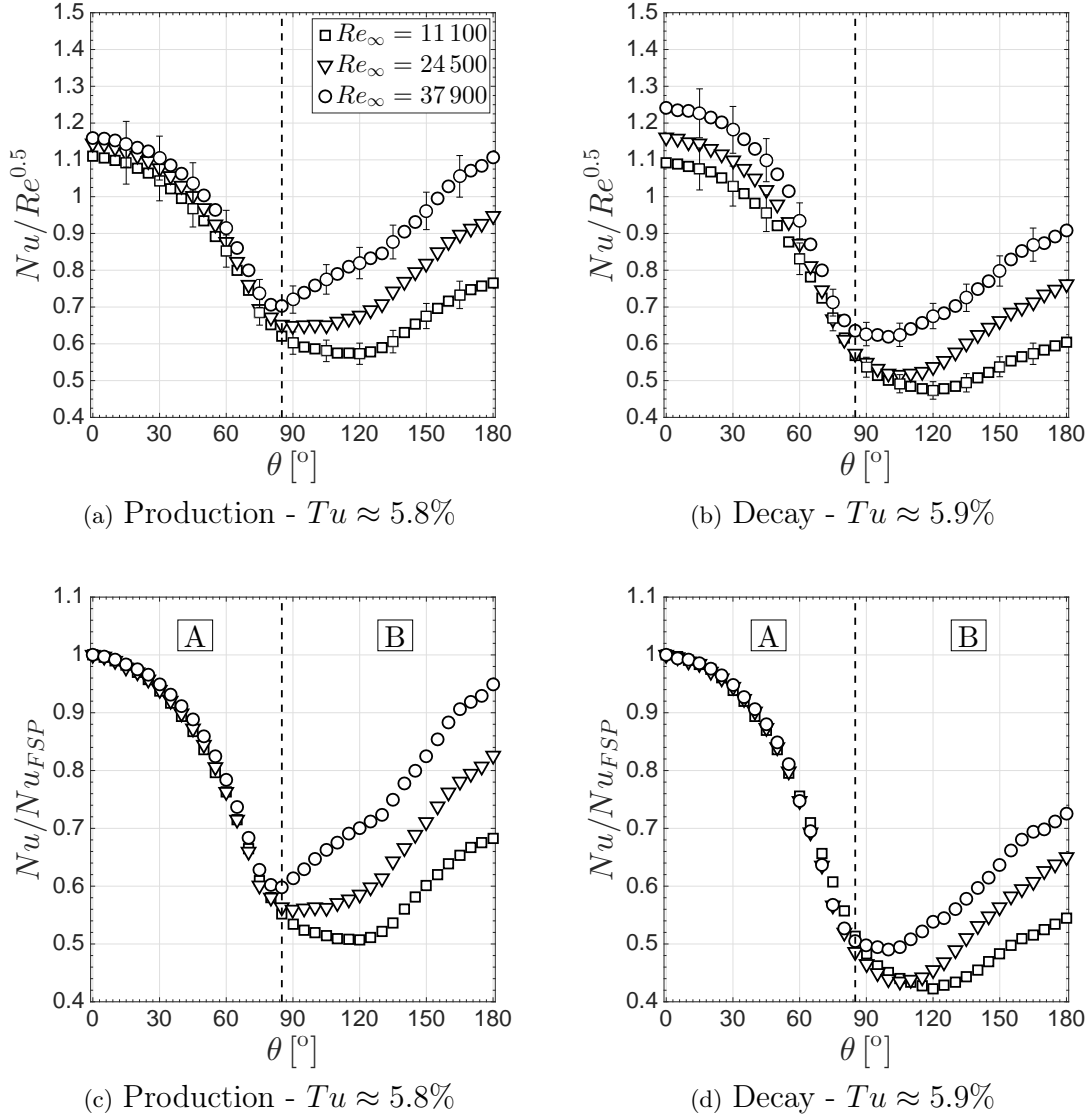


Fig. 7: Angular profiles of $Nu/Re^{0.5}$ (top) and of Nu/Nu_{FSP} (bottom) for FSG17 in the production region at $x/H = 1.28$ (left) and in the decay region at $x/H = 5.12$ (right). The vertical dashed lines divide the angular domain in the boundary layer region (region A, $0^\circ < \theta < 85^\circ$) and in the wake region (region B, $85^\circ < \theta < 180^\circ$). The error bars in (a) and (b) indicate the experimental errors evaluated via a single-sample uncertainty analysis with 95% confidence intervals.

lower in the production region. One would therefore expect higher heat transfer rates in the production region than in the decay region. It is possible that the large-scale anisotropy and the in-homogeneity of the flow in the production region of grid-generated turbulence (see e.g. Hurst and Vassilicos, 2007; Laizet and Vassilicos, 2011; Gomes-Fernandes et al., 2015) affect the heat transfer from the cylinder. However the results of Van Fossen et al. (1995) seem to indicate that a large-scale anisotropy of the approaching turbulent flow causes higher values of $Nu/Re^{0.5}$ in the proximity of the FSP of the cylinder with respect to the isotropic case whereas for SSG the

opposite occurs. The presence of multiple geometric iterations for FSG17 and the large values of x^* for both SSG and FSG17 might imply that when the cylinder is placed in the production region it is approached by a non uniform flow. However the diameter of the cylinder used in this experiment is kept small so that one can expect that $\partial U/\partial y \times D/U$ is also small in the proximity of the centreline circumference where the heat transfer profiles are measured, y being the spanwise coordinate. Zhou et al. (2014) performed Direct Numerical Simulations (DNS) of the flow downstream of a single square grid and of a fractal square grid, which are similar to the grids SSG and FSG17 used here. Analysis of their results (see Fig. 6 and Fig. 7 of Zhou et al., 2014) reveals that for $-D/2 < y < D/2$ the mean velocity and the turbulence intensity can be considered approximately uniform in the production region of both the single and the fractal square grid at values of x/x^* (or x/x_{peak}) similar to those considered in this paper. One can therefore assume that the centreline circumference of the cylinder used in this experiment is approached by a flow which is reasonably uniform within a distance D when the cylinder is placed in the production region, i.e. at $x/x_{peak} = 0.56$ for SSG and at $x/x_{peak} = 0.50$ for FSG17.

Comparison of the heat transfer profiles for FSG17 in its production region (Fig. 7a) with those in its decay region (Fig. 7b) reveals that, differently from SSG, the values of $Nu/Re^{0.5}$ on the front of the cylinder (region A) are not significantly lower in the production region than in the decay region. Considering the experimental uncertainty of the experiments (shown with error bars in Figs. 7a,b), one can argue that for FSG17 the values of $Nu/Re^{0.5}$ in region A of the cylinder are similar between production (Fig. 7a) and decay (Fig. 7b). However it is important to note that, for the higher Re_∞ , $Nu/Re^{0.5}$ on the front of the cylinder is higher in the production region of FSG17 (Fig. 7a) than in the production region of SSG (Fig. 6a). This happens despite x/x_{peak} being comparable for the selected locations and despite Tu being appreciably higher for SSG than for FSG17.

When comparing SSG and FSG17 in their production regions, it is relevant to consider an important difference between flow downstream of these two grids. Fig. 8 shows contour plots of the power spectral density E_u of u , normalised by $u'^2/(U_\infty/H)$, in the frequency domain f , normalised by U_∞/t_0 , along the centreline for $0.3 \leq x/H \leq 3.5$ and $0.08 \leq ft_0/U_\infty \leq 0.3$. When considering the locations for the cylinder placed in the production region where the heat transfer profiles are compared (indicated by the vertical dashed lines in Fig. 8), one can see that for SSG (Fig. 8a) the contribution to the total turbulent kinetic energy u'^2 is mostly concentrated in a narrow range of frequencies across $ft_0/U_\infty \approx 0.19$, suggesting it is a result of strong vortex

Grid	x/H	x/x_{peak}	Re_∞	$f_{sh}t_0/U_\infty$	$E_{sh}/U^2 \times 10^3$	E_{sh}/u'^2
SSG	0.75	0.56	11 100	0.19	6.3	0.6
			37 900	0.19	6.1	0.7
FSG17	1.28	0.50	11 100	0.13	0.8	0.2
			37 900	0.13	0.8	0.2

Tab. 3: Vortex shedding frequency and vortex shedding energy (for $\Delta f/f_{sh} = 0.5$) in the production regions of SSG (at $x/x_{peak} = 0.56$) and of FSG17 (at $x/x_{peak} = 0.50$).

shedding from the bars of the grid. For FSG17 (Fig. 8b) most of the energy is not associated with the shedding frequency of the large bars, $f_{sh}t_0/U_\infty \approx 0.13$, but is more distributed across the frequencies, i.e. it is due to the stochastic component of the velocity fluctuations, not to the shedding. As already shown in Melina et al. (2016), the higher Tu for SSG than for FSG17 in the production region can be explained by a more intense vortex shedding contribution (periodic component of the velocity fluctuations) for SSG. For FSG17 the effect of vortex shedding is less intense along the centreline and it disappears more quickly in terms of x/H as Fig. 8 clearly shows. Tab. 3 reports the values of the frequency, f_{sh} , and of the energy, E_{sh} , associated with the vortex shedding from the largest bars of the grids in the production region of SSG and FSG17. These calculations are obtained from the hot-wire measurements performed (without the cylinder in place) at $Re_\infty = 11\,100$ ($U_\infty = 5\text{ m s}^{-1}$) and at $Re_\infty = 37\,900$ ($U_\infty = 17\text{ m s}^{-1}$) at the positions of the cylinder in the production region where the heat transfer profiles are considered in Fig. 6 for SSG and in Fig. 7 for FSG17. The vortex shedding energy E_{sh} is computed with:

$$E_{sh} = \int_{f_{sh}-\Delta f/2}^{f_{sh}+\Delta f/2} E_u(f) df, \quad (2)$$

where $\Delta f/f_{sh} = 0.5$ for both SSG and FSG17 as done in Melina et al. (2016). As anticipated in Section 3.1 one can see (Tab. 3) that for similar values of x/x_{peak} ($x/x_{peak} = 0.56$ for SSG and $x/x_{peak} = 0.50$ for FSG17) and for the same choice of $\Delta f/f_{sh}$, both the magnitude of E_{sh}/U^2 and that of E_{sh}/u'^2 are noticeably lower for FSG17 than for SSG, thus further confirming that the shedding from the largest bars of the fractal grid is less energetic than for the single square grid used here.

One may ask if the presence of a strong vortex shedding in the production region (originating from the large bars of the grids) can explain why, especially for SSG, the heat transfer on the front of the cylinder is lower in the production region than in the decay region, where Tu is the same but the shedding signature on the energy spectrum of u has almost vanished. For this purpose it is useful to consider the model suggested by Dullenkopf and Mayle (1995) which

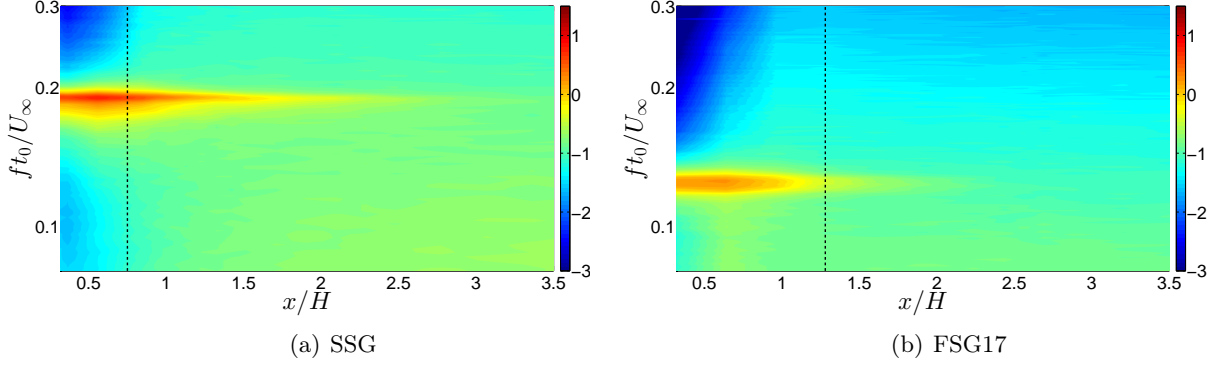


Fig. 8: Contours of the power spectral density E_u normalised by $u'^2 / (U_\infty / H)$ (in logarithmic scale) for SSG (a) and for FSG17 (b) along the centreline obtained without the cylinder in place. The vertical dashed lines identify the locations $x/H = 0.75$ ($x/x_{peak} = 0.56$) in (a) and $x/H = 1.28$ ($x/x_{peak} = 0.50$) in (b) in the turbulence production region where the heat transfer measurements on the cylinder are performed; $Re_\infty = 37\,900$.

introduced the idea of an “effective” turbulence intensity. Dullenkopf and Mayle (1995) developed a heat transfer model for the FSP by assuming that a laminar boundary layer, and so the heat transfer process on the front of a cylinder, is more sensitive to disturbances with frequency $f \in [f_\lambda - \Delta f/2, f_\lambda + \Delta f/2]$, where f_λ is a dominant “effective” frequency, and $\Delta f/f_\lambda \ll 1$. This model assumes that velocity fluctuations at high frequencies ($f \gg f_\lambda$) are not effective since they are damped by diffusive effects, while those at low frequencies ($f \ll f_\lambda$) are also not effective since they appear as quasi-steady. One can have a rough estimate of f_λ to check if (i) $f_\lambda \gg f_{sh}$ and if (ii) the energy associated to f_λ is lower in the production region than in the decay region, especially for SSG where strong vortex shedding is evident on the spectrum of u (see Fig. 8a). Dullenkopf and Mayle (1995) calibrated their model on sets of experimental data and suggested that:

$$f_\lambda \approx 0.02 U / \delta, \quad (3)$$

where δ is the boundary layer thickness. Following Dullenkopf and Mayle (1995), for a stagnation flow on a cylinder one can estimate δ from $\delta/D = 2.4 / (a_1 Re)^{0.5}$, where a_1 is the strain rate parameter, $a_1 = |\partial U_{app} / \partial x| D / U$, and U_{app} is the velocity of the flow approaching the cylinder. In absence of measurements of the strain rate at the FSP, the parameter a_1 is taken to be $a_1 = 4$ (which is the value for a potential flow) for the purpose of our estimates. Following the hypothesis of the model of Dullenkopf and Mayle (1995), the “effective” turbulence kinetic energy can be computed as:

$$u_{eff}^2 = \int_{f_\lambda - \Delta f/2}^{f_\lambda + \Delta f/2} E_u(f) df, \quad (4)$$

Grid	Re_∞	Tu [%]		f_λ/f_{sh}		$Tu_{eff} \times 10^3$	
		PROD	DEC	PROD	DEC	PROD	DEC
SSG	11 100	9.9	9.6	14.8	11.9	4.1	6.4
	37 900	9.6	10.0	28.1	21.9	2.8	5.2
FSG17	11 100	5.6	5.8	11.4	9.0	3.4	3.3
	37 900	6.0	6.0	21.0	16.2	2.6	2.8

Tab. 4: Estimates of the effective frequency (normalised with the shedding frequency of the grids) and of the effective turbulence intensity (for $\Delta f/f_\lambda = 0.05$) for SSG and FSG17 in the production (PROD) region ($x/H = 0.75$ for SSG and $x/H = 1.28$ for FSG17) and in the decay (DEC) region ($x/H = 3.07$ for SSG and $x/H = 5.12$ for FSG17).

where Δf is chosen by imposing $\Delta f/f_\lambda = 0.05$ in our calculations. Next, an “effective” turbulence intensity can be computed as $Tu_{eff} = u'_{eff}/U$.

The estimates of f_λ and Tu_{eff} are reported in Tab. 4 for the positions of the cylinder where the heat transfer profiles are compared in Fig. 6 for SSG and in Fig. 7 for FSG17. It is important to observe that, for the range of Re_∞ investigated here, f_λ is well above f_{sh} , especially for SSG and more so for higher Re_∞ . Note in fact that f_λ/f_{sh} increases with Re according to $f_\lambda/f_{sh} \propto Re^{0.5} U/U_\infty$, provided that f_{sh}/U_∞ is invariant with U_∞ for each grid, as verified here (see Tab. 3) and in Melina et al. (2016), and if a_1 is assumed constant. Looking at the estimates of Tu_{eff} in Tab. 4, it is observed that, for SSG, Tu_{eff} is noticeably lower in the production region than in the decay region and that the difference increases with Re_∞ . For $Re_\infty = 37900$, the estimated value of Tu_{eff} in the production region of SSG is about 45% lower than in the decay region. Given these results, the presence of intense vortex shedding from the bars of SSG can explain why $Nu/Re^{0.5}$ on the front of the cylinder (boundary layer region) is lower in the production region (Fig. 6a) than in the decay region (Fig. 6b), despite the overall turbulence intensity being approximately the same. In the production region of SSG, a big contribution of the turbulent kinetic energy is localised around the shedding frequency f_{sh} of the bars, which is far from the frequency f_λ , and therefore may not be effective in enhancing the heat transfer across the laminar boundary layer which develops on the front section of the cylinder. It is important to consider that for Reynolds numbers lower than in this experiment, the shedding frequency f_{sh} of the grid’s bars can have a value close to f_λ ($f_\lambda/f_{sh} \propto Re^{0.5}$). One can speculate that in this case the heat transfer in the boundary layer region of the cylinder (front of the cylinder) could be increased by the presence of vortex shedding from the grid, as opposed to what is observed for the range of Re tested in this experiment. In a similar way it is suggested that, for a given Re , one could also tune the value of f_{sh} to be close to that of f_λ by properly selecting the value of t_0 of the largest bars of the grid, therefore causing higher values of Tu_{eff} (and so higher

heat transfer rates) in the production region via vortex shedding, as opposed to what occurs for the range of geometric parameters used here. Dedicated experiments and numerical simulations could explore these suggested scenarios.

In contrast to SSG, the estimated values of Tu_{eff} are found to be approximately the same in the production region and in the decay region of FSG17 (see Tab. 4). These values are lower, or at least the same, when compared to the production region of SSG. Despite that, for the highest Re_∞ , $Nu/Re^{0.5}$ on the front of the cylinder is higher in the production region of FSG17 (Fig. 7a) than in the production region of SSG (Fig. 6a). A possible explanation for this can be provided by the following argument. When the cylinder is placed in the production region ($x/x_{peak} < 1$), the wakes originating from the largest bars of the grid have not completely merged (this occurs for $x/x_{peak} \approx 1$, as explained in Mazellier and Vassilicos, 2010). As a result the flow is more intermittent (i.e. the velocity signal exhibits an alternation between turbulent and potential flow behaviour) in the turbulence production region, as recently shown by the DNS results of Zhou et al. (2016) for the case of a single square grid. Van Dresar and Mayle (1989) studied the mass transfer from a cylinder with an incident wake flow generated by a smaller cylinder. The mass transfer coefficients were measured for different lateral positions of the cylinder in the wake. Their study found that when the cylinder had an offset with respect to the wake centreline, the mass transfer values on its front part were better correlated with an intermittency parameter rather than with the turbulence intensity Tu . In particular a higher intermittency of the flow was found to mitigate the effect of Tu in enhancing the mass transfer. One might infer that the flow is less intermittent in the production region of FSG17 than of SSG at a similar x/x_{peak} , this leading to higher heat transfer rates for FSG17, consistently with the previous intermittency argument. The reason for this can be related to the presence of the smaller geometrical iterations in FSG17, i.e. to its multi-scale design, as these iterations are not present in SSG. One has to consider that, for FSG17, the wake interaction length scales $x_j^* = L_j^2/t_j$ related to the smaller iterations ($j = 1, 2, 3$) have a lower value than $x^* = L_0^2/t_0$ which is related to the first iteration. Given that $x_{peak}/x^* \approx 0.4$ for FSG17 (as also found in Laizet et al., 2015), one can conclude that despite the wakes from the largest iteration ($j = 0$) having not met at $x/x_{peak} = 0.5$ (where the considered heat transfer profiles are measured), the wakes from smaller iterations (at least from iterations 2 and 3) have already merged. This would be consistent with a lower intermittency of the flow in the production region of FSG17 than in the production region of SSG for the same x/x_{peak} .

By comparing the angular distributions of Nu/Nu_{FSP} for FSG17 in the production region (Fig. 7c) with those in the decay region (Fig. 7d), it is clear that the heat transfer profiles are significantly different over the rear of the cylinder (region B). In particular the values of Nu/Nu_{FSP} are consistently higher in the production region than in the decay region for every considered Re_∞ . For $Re_\infty = 37900$ the value of Nu_{RSP}/Nu_{FSP} in the production region of FSG17 is about 30% higher than in the decay region, where Tu is the same. One might argue that this effect is just due to the higher values of the local Re in the production region. Indeed, as already mentioned, for the same Re_∞ the value of U (and so Re) is higher in the production region. However, this effect, by itself, cannot explain the higher heat transfer recovery in the production region. In fact, it is noteworthy that Nu_{RSP}/Nu_{FSP} for FSG17 at $Re_\infty = 24500$ in the production region is about 14% higher than Nu_{RSP}/Nu_{FSP} at $Re_\infty = 37900$ in the decay region. This effect is not specific to FSG17. Comparison of Fig. 6c with Fig. 6d shows that over the rear of the cylinder (wake region), the heat transfer recovery is higher in the production region than in the decay region of SSG too. The profiles of Nu/Nu_{FSP} are shown at all the considered streamwise locations for both FSG17 (Fig. 9) and for SSG (Fig. 10). It is possible to see that, for both FSG17 and SSG, Nu/Nu_{FSP} in the production region ($x/H < 2.56$ for FSG17 and $x/H < 1.33$ for SSG) is higher than for all measurement locations in the decay region. The values of Nu/Nu_{FSP} in region B generally decrease with x/H , with this effect being more discernible for FSG17. For SSG, the heat transfer profiles are more affected by the presence of the previously mentioned “bump” around $\theta = 120^\circ$, especially for the higher Re_∞ . For SSG the magnitude of this localised increase of Nu is higher for the positions closer to $x_{peak}/H = 1.33$, where Tu is maximum, and decreases with x/H . On the contrary for FSG17 at the same Re_∞ , this feature is much less pronounced, possibly as a result of the lower Tu (Sanitjai and Goldstein, 2001). However given the distributions of Nu/Nu_{FSP} , one can conclude that for both grids the contribution of the backward section of the cylinder to the average \overline{Nu} reduces for increasing x/H .

Since in this experiment no velocity measurements are performed in the near-wake of the cylinder, no definitive physical explanations can be provided for the observed results on the back of the cylinder. However some reasonable arguments can be made. As mentioned in Section 3.2, the heat transfer recovery on the rear portion of the cylinder is dominated by wake effects and in particular, for $\theta > 130^\circ$, it increases due to the periodic contribution of the vortices shed from the cylinder (vortex shedding). This effect becomes more important as the length of the vortex

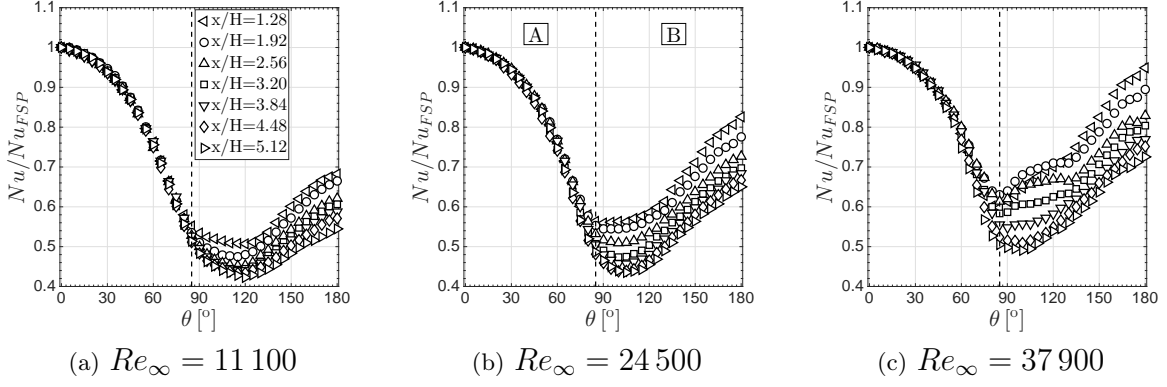


Fig. 9: Angular profiles of Nu/Nu_{FSP} for FSG17 at increasing values of x/H . The vertical dashed lines divide the angular domain in the boundary layer region (region A, $0^\circ < \theta < 85^\circ$) and in the wake region (region B, $85^\circ < \theta < 180^\circ$).

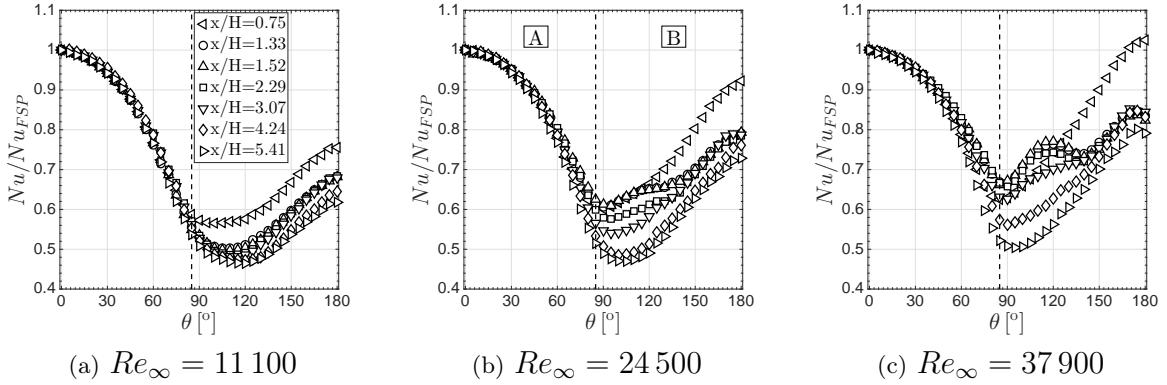


Fig. 10: Angular profiles of Nu/Nu_{FSP} for SSG at increasing values of x/H . The vertical dashed lines divide the angular domain in the boundary layer region (region A, $0^\circ < \theta < 85^\circ$) and in the wake region (region B, $85^\circ < \theta < 180^\circ$).

formation region decreases (Sanitjai and Goldstein, 2004). One can infer that when the cylinder is placed in the production region, the length of the vortex formation region is lower than in the decay region and this induces a higher recovery of Nu with respect to Nu_{FSP} . This effect can be attributed to several combined factors, such as the higher local Re and the lower L_u/D in the production region. The local Re decreases with x/H while L_u/D increases, differently from Tu which instead does not vary monotonically with x/H . In fact, Torii and Yang (1993) showed experimentally that Nu_{RSP} was anti-correlated with L_u/D . This could in part explain the results found for FSG17 and SSG on the back of the cylinder given that L_u/D in the production region is lower than in the decay region. Note that while the trend of L_u/D can not explain the heat transfer results on the front of the cylinder in the production region, it is consistent with the results observed on the rear of the cylinder. Again, it is important to consider that in the production region the wakes originating from the largest bars of FSG17 and SSG will not have

fully merged. One cannot exclude that when the cylinder is placed in the production region, an interaction between the wakes shed from the grid and the wake of the cylinder is likely to occur, almost certainly affecting the heat transfer distribution over the rear of the cylinder and possibly inducing a reduction of the vortex formation length downstream of the cylinder. Future dedicated experiments or numerical simulations could be performed to assess this hypothesis.

Before continuing with the analysis of results, it is useful to briefly summarize the main differences observed between the heat transfer profiles measured in the production region ($x/x_{peak} < 1$) and those in the decay region ($x/x_{peak} > 1$). For SSG it is found that the Frossling number $Nu/Re^{0.5}$ in region A of the cylinder (boundary layer region) is lower in the production region than in the decay region for the same Tu . This was explained by the presence of clear and intense vortex shedding in the production region of SSG. For FSG17 the shedding from the large bars of the grid is noticeably weaker than for SSG at a similar x/x_{peak} . As a result, for FSG17 the values of $Nu/Re^{0.5}$ in region A are not very different between production and decay and are higher than in the production region of SSG. For both SSG and FSG17 it is found that Nu/Nu_{FSP} in region B of the cylinder (wake region) is higher in the production region than in the decay region. This is suggested to be due to a combined effect of (i) higher centreline values of Re , (ii) lower values of L_u/D in the production region, and (iii) a possible interaction between the wakes of the largest bars of the grids and the wake of the cylinder when the latter is placed in the production region.

3.3.2 Effect of the integral length scale in the turbulence decay region

The effect of the integral length scale ratio L_u/D on heat transfer is investigated using the results for the FSP obtained in the turbulence decay regions of the grids. The values of Tu , Re and L_u/D considered here are based on the hot-wire results shown in Fig. 3 which were obtained when the cylinder was not in place for $Re_\infty = 11\,100$ and for $Re_\infty = 37\,900$. For the heat transfer measurements performed at $Re_\infty = 24\,500$, we consider the average values of U/U_∞ , Tu and L_u/D , between those at the lowest Re_∞ and those at the highest Re_∞ given that they do not significantly change with Re_∞ (see Section 3.1).

Fig. 11a shows values of $Nu_{FSP}/Re^{0.5}$ plotted against the turbulence parameter $Tu Re^{0.5}$, together with the empirical correlation of Lowery and Vachon (1975). For FSG17 and SSG the values of $Nu_{FSP}/Re^{0.5}$ follow the same trend and are both consistently lower than for RG60. This can be explained by an effect of L_u/D which for FSG17 and SSG is higher than for RG60,

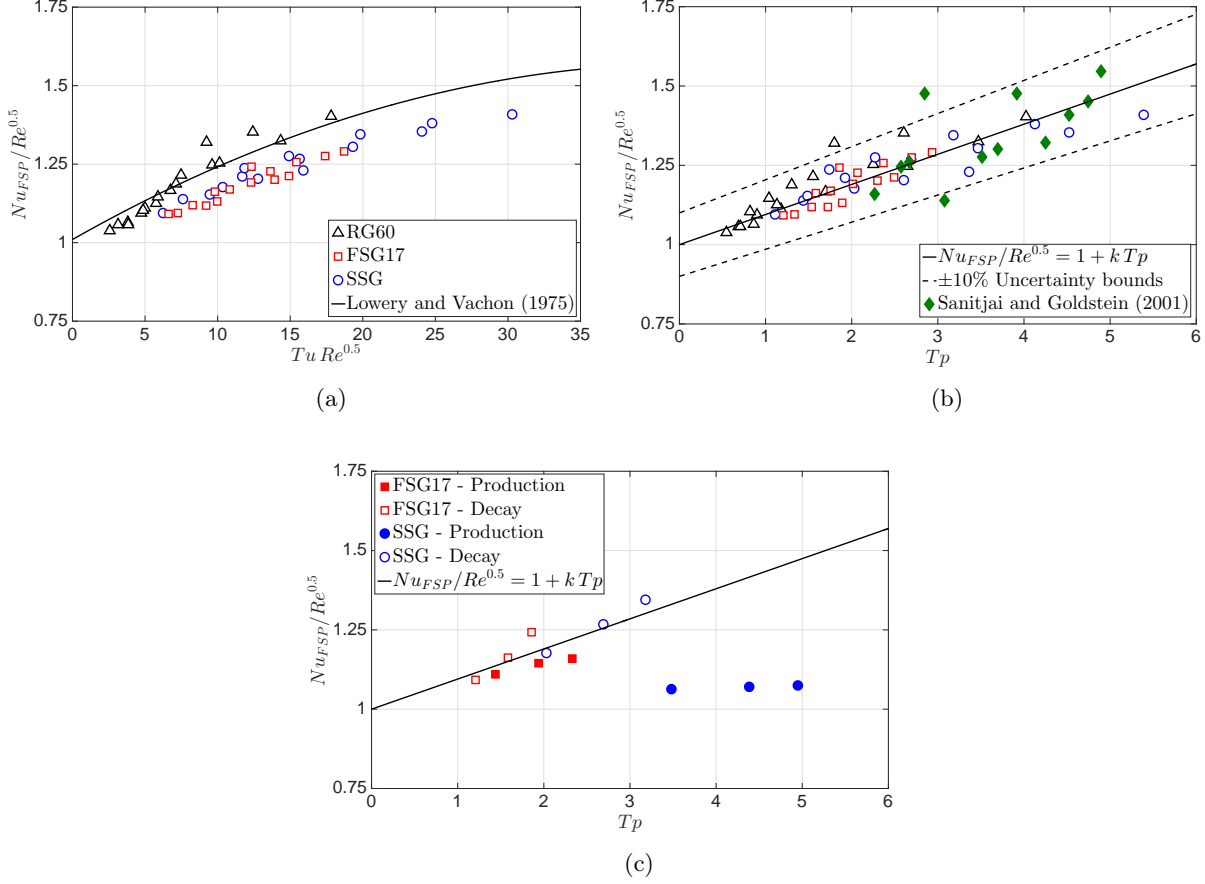


Fig. 11: Heat transfer data at the FSP in the turbulence decay regions of the grids as a function of $TuRe^{0.5}$ (a) and of $Tp = Tu Re^{1/3} (L_u/D)^{-1/3}$ (b). Heat transfer data at the FSP in the turbulence production region (filled symbols) and in the turbulence decay region (empty symbols) of SSG and of FSG17 as a function of Tp (c) at the locations considered in Fig. 6 and in Fig. 7.

as seen in Section 3.1 (Fig. 3c). Under the present experimental conditions, the higher integral length scale for the two grids with higher L_0 tends to reduce the heat transfer augmentation at the FSP.

Previous measurements in grid-decaying turbulence were used to develop empirical correlations which predict $Nu_{FSP}/Re^{0.5}$ as a function of Re , Tu , and L_u/D . Dullenkopf and Mayle (1995) developed a correlation in the form $Nu_a Pr^{-0.37} \propto Tu_\lambda$, where $Nu_a = Nu_{FSP}/(a_1 Re^{0.5})$ and Pr is the Prandtl number of the fluid, $Pr = 0.7$ here. The correlating parameter Tu_λ is a function of Re , Tu , L_u/D and of the strain rate parameter a_1 : $Tu_\lambda = Tu_a L_a^{0.5}/(1 + 0.004 L_a^2)^{5/12}$ where $Tu_a = Tu (Re/a_1)^{0.5}$ and $L_a = L_u (a_1 Re)^{0.5}/D$. A result of the model of Dullenkopf and Mayle (1995) is that there is an optimal value of L_u/D , $(L_u/D)_{opt}$, for which the heat transfer augmentation at the FSP is maximum. This reflects the idea that turbulent scales that are too small or too big are not effective in enhancing the heat transfer. Assuming the value

$a_1 = 4$ (value for a potential flow), the model predicts $(L_u/D)_{opt} Re^{0.5} \approx 10$, consistent with the results of Yardi and Sukhatme (1978) for Nu_{FSP} , and those of Zukauskas et al. (1993) for \overline{Nu} . For $L_u/D \gg (L_u/D)_{opt}$ and for a constant value of a_1 , the parameter Tu_λ reduces to the turbulence parameter $Tp = Tu Re^{1/3} (L_u/D)^{-1/3}$, so that the heat transfer data can be correlated in the simpler form $Nu_{FSP}/Re^{0.5} \propto Tp$. This is the case of the present experiment as in the turbulence decay regions of the grids it is always the case that $(L_u/D) Re^{0.5} > 10$ (in fact $48 < (L_u/D) Re^{0.5} < 317$) so that increasing values of L_u/D are expected to cause a reduction of the heat transfer coefficient at the FSP. For this reason, in the decay regions the values of $Nu_{FSP}/Re^{0.5}$ can be correlated as a linear function of Tp , $Nu_{FSP}/Re^{0.5} = 1 + kTp$, with $k = \text{constant}$ and where the ordinate-intercept is 1 as it represents the value of $Nu_{FSP}/Re^{0.5}$ for laminar free-stream conditions (see Section 3.2). The data for RG60, FSG17, and SSG in their turbulence decay regions are shown in Fig. 11b in terms of the Frossling number $Nu_{FSP}/Re^{0.5}$ against the correlating parameter Tp , together with a curve representing a fit of the data and $\pm 10\%$ uncertainty limits. The mass transfer results (converted to heat transfer data) of Sanitjai and Goldstein (2001) are also shown for reference in the range of Tp covered in this experiment, $0 < Tp < 5.4$.

Fig. 11c shows the values of $Nu_{FSP}/Re^{0.5}$ as a function of Tp for FSG17 and for SSG in their turbulence production region and in their turbulence decay region for the locations previously considered in Figs. 7 and 6. It is useful to recall that in these positions Tu is approximately the same in the production region and in the decay region of each grid and that it is higher for SSG. The values of Tp in the SSG's production region are noticeably higher than in the SSG's decay region because of the large difference in L_u/D at the cylinder positions considered (see Fig. 3c). As seen in the previous section, for FSG17 the values of $Nu_{FSP}/Re^{0.5}$ in the production region are marginally lower than in the decay region, while for SSG the difference is significantly more accentuated. Note that Dullenkopf and Mayle (1995) obtained the functional dependence of Tu_λ (and so of Tp) on Tu and L_u/D by assuming a von Karman spectrum model for E_u . This model cannot be used to fit a spectrum with a marked vortex shedding signature, as is the case for SSG in the production region position considered in Fig. 11c.

It is interesting to note that Tp is similar to the parameter $TRL = Tu Re^{5/12} (L_e/D)^{-1/3}$ developed by Ames and Moffat (1990), as already pointed out in Dullenkopf and Mayle (1995). However it is important to stress that while the parameter Tp makes use of the integral length scale L_u , the parameter TRL is based on L_e , which is a dissipation length scale, $L_e \propto u'^3/\epsilon$.

Some investigations have used L_u to correlate heat transfer data (e.g. Van Fossen et al., 1995; Dullenkopf and Mayle, 1995; Sanitjai and Goldstein, 2001; Nix et al., 2007) while others have used L_e (e.g. Hancock and Bradshaw, 1983; Ames and Moffat, 1990; Ames, 1997; Gandavarapu and Ames, 2013). It must be emphasised that there is no difference if $C_\epsilon = \text{constant}$ in the decay region of the turbulence-generators, given that $L_e \propto L_u/C_\epsilon$. However when $C_\epsilon \neq \text{constant}$, as has been observed to be the case for FSG17 and SSG in their decay regions (see Section 3.1), one may ask whether the most appropriate scale to model Nu_{FSP} is L_u or L_e , i.e. whether C_ϵ has a role on heat transfer enhancement. The data collected in this experiment cannot address this point as one should cover an extensive range of Re , Tu , L_u/D and C_ϵ . It is also critical that the frequency response of the hot-wire is high enough to accurately compute the dissipation even for the higher Re_∞ . The important point to make here is that the geometries of FGS17 and SSG magnify the physical extent of the $C_\epsilon \neq \text{constant}$ turbulence decay region (see Fig. 3d), and therefore open new research questions on the role of additional turbulence parameters of the flow on heat transfer enhancement. Note in fact that $C_\epsilon \propto Re_G^{1/2}/Re_\lambda$ (see Vassilicos, 2015), where Re_G is an inlet Reynolds number based on U_∞ and a characteristic length scale of the grid and Re_λ is based on the local u' and Taylor length scale λ . This means that if the value of C_ϵ plays a role on the heat transfer values, both the local Taylor length scale and an inlet scale determined by the geometry of the turbulence generator might also need to be taken into account.

3.3.3 Average heat transfer

The evolution of the circumferentially averaged Nusselt number \overline{Nu} along the centreline is shown in Fig. 12 (left side of the plot) for the three grids used in this experiment. It is evident that for the selected streamwise positions of the cylinder, the heat transfer is appreciably higher for FSG17 and SSG than for RG60. This trend appears to be independent of Re_∞ over the range studied here. For example, at $Re_\infty = 37\,900$, the value of \overline{Nu} at $x/H = 3$ for FSG17 and SSG is respectively about 29% and 33% higher than that for RG60. Note that the values of \overline{Nu} for FSG17 are slightly lower or very close to those of SSG. This happens despite the values of Tu for FSG17 being lower than for SSG (see Fig. 3b) and L_u/D being instead comparable (see Fig. 3c). A possible explanation of this feature is that the local higher Re for FSG17 counter-balances the lower Tu , resulting in similar heat transfer coefficients for FSG17 and SSG. When the average Frossling number $\overline{Nu}/Re^{0.5}$ is considered (Fig. 12, right side of the plot), one can see this is indeed lower for FSG17 than for SSG, due to the higher local mean velocity. It is interesting

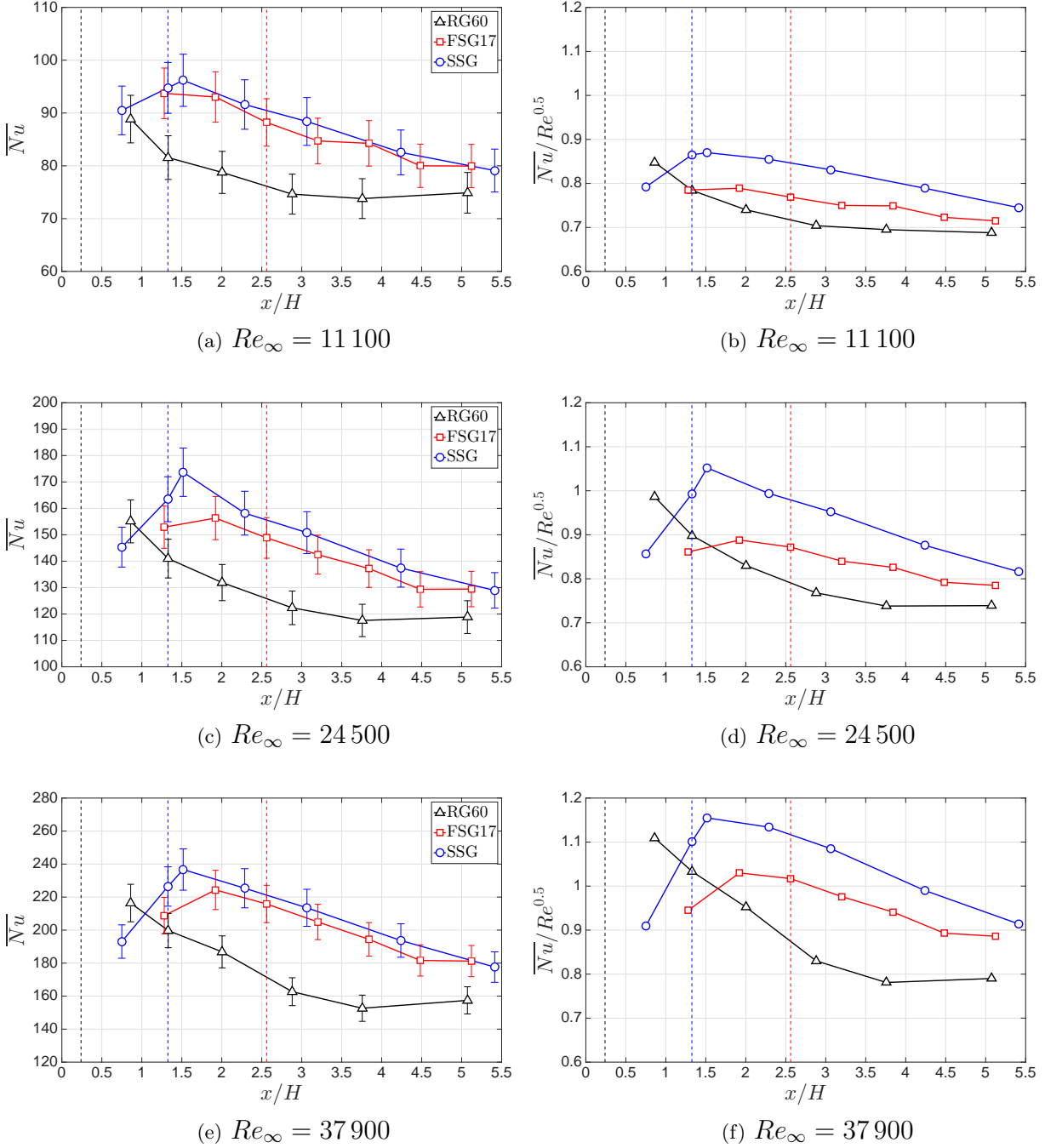


Fig. 12: Centreline streamwise evolution of \overline{Nu} (left) and of $\overline{Nu}/Re^{0.5}$ (right) for RG60, FSG17 and SSG at different Re_∞ . The vertical dashed lines indicate the position of x_{peak} for each grid (black for RG60, red for FSG17 and blue for SSG). The error bars in (a), (c) and (d) indicate the experimental errors evaluated via a single-sample uncertainty analysis with 95% confidence intervals.

to note that for FSG17 the maximum average heat transfer seems to occur in the production region ($x/H = 1.92$), which is where the local Re and the contribution of the backward part of the cylinder to \overline{Nu} are higher (see Fig. 7 and Fig. 9).

An important conclusion here is that for large distances from the grid, the average heat

transfer on the cylinder is augmented more if the fractal grid FSG17 or the single square grid SSG are used in place of the regular square-mesh grid RG60 tested here. This is different from what was found in the case of an impinging jet (Cafiero et al., 2014), where the performance of a fractal grid insert (in terms of heat transfer enhancement) was appreciably higher than that of a regular grid insert for low nozzle-to-plate distances, i.e. for positions closer to the grid. It is important to stress that in the present case FSG17 and SSG have a smaller blockage ratio σ_g than RG60. This means that the heat transfer can be augmented more efficiently by using FSG17 or SSG, i.e. it is possible to achieve higher heat transfer coefficients together with a lower σ_g and therefore with a lower static pressure drop across the grid (see Melina et al., 2016). This differs from the results of Quintino (2012) where, for the geometries of the grids used in his experiment (grids made of two vertical strips), the augmentation of \overline{Nu} increased with σ_g .

The higher values of \overline{Nu} for FSG17 and SSG compared to RG60 can be explained mainly by the higher values of Tu in their turbulence decay regions. However, if L_u/D is significantly larger, obtaining a higher heat transfer coefficient with a higher Tu cannot be taken for granted. The geometries of both FSG17 and SSG are characterised by a high value of L_0 and as a result the values of L_u/D are increased with respect to RG60. As previously seen for the FSP, large values of L_u tend to reduce the heat transfer. This means that if L_u becomes too large, the values of Nu_{FSP} , and so those of \overline{Nu} , could remain low despite a high turbulence intensity. However the results of the present experiment show that for FSG17 and SSG, the increase of L_u/D is moderate enough for average heat transfer levels to be noticeably higher than those with RG60 at a large distance from the turbulence-generator. The geometric parameters of the grids, mainly x^* and t_0/L_0 , can be tuned in order to prescribe desired levels of turbulence intensity and so desired levels of heat transfer augmentation while keeping the blockage of the grid low, thus limiting the static pressure drop across the grid.

4 Conclusions

Heat transfer measurements were performed around the centreline circumference of a cylinder in crossflow placed in a wind tunnel at $Re_\infty = 11\,100, 24\,500, 37\,900$. The cylinder was positioned at several streamwise distances x from 3 turbulence-generating grids with different geometries and blockage ratios σ_g : a regular grid (RG60), a fractal square grid (FSG17) and a single square grid (SSG). The turbulent flow downstream of the grids was first characterised without the cylinder

in place with hot-wire anemometry measurements along the centreline for $Re_\infty = 11\,100$ and $Re_\infty = 37\,900$. In the turbulence decay region ($x > x_{peak}$) the values of Tu for FSG17 and SSG are higher than those for RG60 ($\sigma_g = 32\%$), despite σ_g being lower for FSG17 ($\sigma_g = 25\%$), and for SSG ($\sigma_g = 20\%$). However, in the same region, FSG17 and SSG also produce greater values of the integral length scale L_u than RG60 because of their larger value of L_0 . The maximum turbulence intensity Tu_{peak} on the centreline is higher for SSG than for FSG17. This is mostly due to a more intense vortex shedding from the bars of SSG.

Thanks to a higher value of their wake interaction length scale x^* , SSG and more importantly FSG17 enlarge the physical extent of the turbulence production region ($x < x_{peak}$) with respect to RG60. For FSG17 and SSG, the angular heat transfer profiles are measured with the cylinder placed in the production region and are compared to those in the decay region, in positions where Tu is approximately the same as in the production region locations. For SSG, the values of $Nu/Re^{0.5}$ on the front of the cylinder (boundary layer region) are lower in the production region than in the decay region. This is explained by considering that in the production region of SSG, a great contribution to the turbulent kinetic energy is due to the vortex shedding from its bars. For the range of geometric and inlet conditions of the present experiment, this causes the values of Tu_{eff} , and so those of $Nu/Re^{0.5}$, to be lower in the production region than in the decay region despite the overall Tu being the same, where Tu_{eff} is the turbulence intensity “effective” in enhancing the heat transfer in a laminar boundary layer which is estimated following the model of Dullenkopf and Mayle (1995). For the higher Re_∞ , the values of $Nu/Re^{0.5}$ on the front of the cylinder are higher in the production region of FSG17 than in the production region of SSG at comparable values of x/x_{peak} , despite Tu being lower for FSG17 and Tu_{eff} being similar. This may be the result of a lower intermittency of the flow in the production region of FSG17 than in the production region of SSG. The ratio Nu/Nu_{FSP} over the rear of the cylinder (wake region) is noticeably higher in the production region than in the decay region, both for FSG17 and for SSG. This result can be explained by (i) higher centreline values of the local Re and (ii) lower values of the integral length scale ratio L_u/D in the production region than in the decay region. Moreover since in the production region the wakes shed from the largest bars of the grid have not fully merged yet, (iii) it is likely that an interaction between the wakes of the grid and the wake of the cylinder occurs, this causing a reduction of the vortex formation length downstream of the cylinder when it is placed in the production region. For the same parameter $Tu Re^{0.5}$, the values of $Nu_{FSP}/Re^{0.5}$ for FSG17 and SSG in their decay regions are approximately the same

but are lower than for RG60, this happening because of a higher L_u/D for FSG17 and SSG than for RG60. For the range of L_u/D investigated in this study, a higher integral length scale in the decay region tends to penalise the heat transfer augmentation.

The streamwise evolution of the centreline circumferentially averaged Nusselt number, \overline{Nu} , is quantified for RG60, FSG17 and SSG. It is found that at a large distance from the turbulence generators in the decay region, the values of \overline{Nu} for both FSG17 and SSG are noticeably higher than those for RG60 at the same x and for the same Re_∞ . This means that, for a large distance from the grid, the heat transfer can be enhanced more efficiently using FSG17 and SSG, i.e. producing a higher \overline{Nu} together with a lower pressure drop across the turbulence generators, as the blockage ratio σ_g for SSG and FSG17 is lower than for RG60. The geometrical design of FSG17 and SSG can be optimised for heat transfer enhancement according to the specific needs. In particular the wake-interaction length scale x^* sets the extent of the production region while the ratio t_0/L_0 affects the maximum Tu . The use of FSG17 allows a highly extended turbulence production region, while still offering high values of Tu in the turbulence decay region. The practical advantage of using FSG17 in place of SSG is that high heat transfer rates from the cylinder can be achieved with a weaker vortex shedding from the grid, therefore with a reduced periodic loading on the turbulence generator.

Acknowledgements

The authors acknowledge support from the EU through the FP7 Marie Curie MULTISOLVE project (Grant No. 317269). J.C.V. also acknowledges the support of an ERC Advanced Grant (Grant No. 320560). This work was presented at the “3rd International Conference on Heat Transfer and Fluid Flow - HTFF’16” (August 22-23, 2016) in Budapest, Hungary (www.internationalaset.com). G.M. wishes to thank F. Giammaria for his help in the set-up of the experiment.

References

- Achenbach, E. (1975). Total and local heat transfer from a smooth circular cylinder in cross-flow at high Reynolds number. *Int. J. Heat Mass Transfer*, 18:1387–1396.
- Ames, F. E. (1997). The influence of large-scale high-intensity turbulence on vane heat transfer. *ASME J. Turbomach.*, 119:23–30.
- Ames, F. E. and Moffat, R. J. (1990). *Heat transfer with high intensity, large scale turbulence:*

- The flat plate turbulent boundary layer and and the cylindrical stagnation point.* PhD thesis, Stanford University, Stanford, CA, US.
- Astarita, T., Cardone, G., and Carlomagno, G. (2006). Infrared Thermography: An optical method in heat transfer and fluid flow visualization. *Opt. Laser Eng.*, 44:261–281.
- Boulos, M. I. and Pei, D. C. T. (1974). Dynamics of heat transfer from cylinders in a turbulent air stream. *Int. J. Heat Mass Transfer*, 17:767–783.
- Cafiero, G., Discetti, S., and Astarita, T. (2014). Heat transfer enhancement of impinging jets with fractal-generated turbulence. *Int. J. Heat Mass Transfer*, 75:173–183.
- Cafiero, G., Discetti, S., and Astarita, T. (2015). Flow field topology of submerged jets with fractal generated turbulence. *Phys. Fluids*, 27:115103.
- Cengel, Y. A. (1998). *Heat Transfer: A Practical Approach.* McGraw-Hill, Boston, Massachusetts.
- Chang, B. H. and Mills, A. F. (2004). Effect of aspect ratio on forced convection heat transfer from cylinders. *Int. J. Heat Mass Transfer*, 47:1289–1296.
- Churchill, S. W. and Bernstein, M. (1977). A correlating equation for forced convection from gases and liquids to a circular cylinder in cross flow. *J. Heat Transfer*, 99:300–306.
- Dullenkopf, K. and Mayle, R. E. (1995). An account of free-stream-turbulence length scale on laminar heat transfer. *ASME J. Turbomach.*, 117:401–406.
- Eckert, E. R. G. (1942). Die Berechnung des Wärmeüberganges in der Laminaren Grenzschicht um Stromter Körper. *VDI-Forschungsheft*, 416:1–24.
- Endoh, K., Tsuruga, H., Hirano, H., and Morihira, M. (1972). Effect of turbulence on heat and mass transfer. *Heat Transfer-Jap. Res.*, 1:113–115.
- Fand, R. M. (1965). Heat transfer by forced convection from a cylinder to water in crossflow. *Int. J. Heat Mass Transfer*, 8:143–158.
- Frössling, N. (1958). Evaporation, heat transfer, and velocity distribution int two-dimensional and rotationally symmetrical laminar boundary-layer flow. Technical report, NACA TM 1432.

- Gandavarapu, P. and Ames, F. E. (2013). The influence of leading edge diameter on stagnation region heat transfer augmentation including effects of turbulence level, scale and Reynolds number. *ASME J. Turbomach.*, 135:011008.
- Gerrard, J. H. (1978). The wakes of cylindrical bluff bodies at low Reynolds number. *Philos. Trans. R. Soc. London A*, 288(1354):351–382.
- Gomes-Fernandes, R., Ganapathisubramani, B., and Vassilicos, J. C. (2012). Particle image velocimetry study of fractal-generated turbulence. *J. Fluid Mech.*, 711:306–336.
- Gomes-Fernandes, R., Ganapathisubramani, B., and Vassilicos, J. C. (2015). The energy cascade in near-field non-homogeneous non-isotropic turbulence. *J. Fluid Mech.*, 771:676–705.
- Goto, S. and Vassilicos, J. C. (2016). Unsteady turbulence cascades. *Phys. Rev. E*, 94:053108.
- Hancock, P. E. and Bradshaw, P. (1983). The effect of free-stream turbulence on turbulent boundary layers. *ASME J. Fluid. Eng.*, 105:284–289.
- Hewitt, G. F. (2008). *Heat Exchanger Design Handbook*. Begell House, New York.
- Hurst, D. and Vassilicos, J. C. (2007). Scalings and decay of fractal-generated turbulence. *Phys. Fluids*, 19(3):035103.
- Kays, W. M., Crawford, M. E., and Weigand, B. (2004). *Convective heat and mass transfer*. McGraw-Hill, 4th edition.
- Kestin, J. and Wood, R. (1971). The influence of turbulence on mass transfer from cylinders. *J. Heat Transfer*, 93C:321–327.
- Kondjoyan, A. and Daudin, J. D. (1995). Effects of free stream turbulence intensity on heat and mass transfers at the surface of a circular cylinder and an elliptical cylinder, axis ratio 4. *Int. J. Heat Mass Transfer*, 38(10):1735–1749.
- Laizet, S., Nedić, J., and Vassilicos, J. C. (2015). The spatial origin of -5/3 spectra in grid-generated turbulence. *Phys. Fluids*, 27:065115.
- Laizet, S. and Vassilicos, J. C. (2011). DNS of Fractal-Generated Turbulence. *Flow Turbul. Combust.*, 87:673–705.

- Lam, K., Wang, F. H., and So, R. M. C. (2012). Three-dimensional nature of vortices in the near wake of a wavy cylinder. *J. Fluid. Struct.*, 19:815–833.
- Lee, Y. and Kakade, S. G. (1976). Effect of peripheral wall conductioun on heat transfer from a cylinder in cross flow. *Int. J. Heat Mass Transfer*, 19:1031–1037.
- Lowery, G. W. and Vachon, R. I. (1975). The effect of turbulence on heat transfer from heated cylinders. *Int. J. Heat Mass Transfer*, 18:1229–1242.
- Mazellier, N. and Vassilicos, J. C. (2010). Turbulence without Richardson-Kolmogorov cascade. *Phys. Fluids*, 22:075101.
- Mehendale, A. B., Han, J. C., and Ou, S. (1991). Influence of high mainstream turbulence on leading edge heat transfer. *J. Heat Transfer*, 113:843–850.
- Melina, G., Bruce, P. J. K., and Vassilicos, J. C. (2016). Vortex shedding effects in grid-generated turbulence. *Phys. Rev. Fluids*, 1:044402.
- Moffat, R. J. (1988). Describing the uncertainties in experimental results. *Exp. Therm. Fluid Sci.*, 1:3–17.
- Nix, A. C., Diller, T. E., and Ng, W. F. (2007). Experimental measurements and modeling of the effects of large-scale freestream turbulence on heat transfer. *ASME J. Turbomach.*, 129:542–550.
- Norberg, C. (1998). LDV-measurements in the near wake of a circular cylinder. In *Proceedings of the 1998 ASME Fluids Engineering Division Summer Meeting*, Washington, DC, FED-Vol. 245, FEDSM98-5202.
- Perkins, H. C. and Leppert, G. (1964). Local heat transfer coefficients on a uniformly heated cylinder. *Int. J. Heat Mass Transfer*, 7:143–158.
- Quintino, A. (2012). Experimental analysis of the heat transfer coefficient enhancement for a heated cylinder in cross-flow downstream of a grid flow perturbation. *Appl. Therm. Eng.*, 35:55–59.
- Sak, C., Liu, R., Ting, D. S., and Rankin, G. W. (2007). The role of turbulence length scale and turbulence intensity on forced convection from a heated horizontal circular cylinder. *Exp. Therm. Fluid Sci.*, 31:279–289.

- Sanitjai, S. and Goldstein, R. J. (2001). Effect of free-stream turbulence on local mass transfer from a circular cylinder. *Int. J. Heat Mass Transfer*, 44:2863–2875.
- Sanitjai, S. and Goldstein, R. J. (2004). Forced convection heat transfer from a circular cylinder in crossflow to air and liquids. *Int. J. Heat Mass Transfer*, 47:4795–4805.
- Sikmanovic, S., Oka, S., and Kondar-Djurdjevic, S. (1974). Influence of the structure of turbulent flow on heat transfer from a single cylinder in a cross flow. In *Proceedings of the 5th International Heat Transfer Conference*, volume 2, pages 320–324.
- Smith, M. C. and Kuethe, A. M. (1966). Effects of turbulence on laminar skin friction and heat transfer. *Phys. Fluids*, 9(12):2337–2344.
- Torii, S. and Yang, W. J. (1993). Effects of the length scale of free-stream turbulence and cylinder size on local heat transfer in laminar separated flows. *Exp. Heat Transfer*, 6(2):175–187.
- Valente, P. C. and Vassilicos, J. C. (2014). The non-equilibrium region of grid-generated decaying turbulence. *J. Fluid Mech.*, 744:5–37.
- Van Der Hegge Zijnen, B. G. (1958). Heat transfer from horizontal cylinders to a turbulent air flow. *Appl. Sci. Res.*, 7A:205–223.
- Van Dresar, N. T. and Mayle, R. E. (1989). A quasi-steady approach of wake effects on leading edge transfer rates. *ASME J. Turbomach.*, 111:483–490.
- Van Fossen, G. J., Simoneau, R. J., and Ching, C. Y. (1995). Influence of turbulence parameters, Reynolds number, and body shape on stagnation-region heat transfer. *J. Heat Transfer*, 117:597–603.
- Vassilicos, J. C. (2015). Dissipation in Turbulent Flows. *Annu. Rev. Fluid Mech.*, 47:95–114.
- Yardi, N. R. and Sukhatme, S. P. (1978). Effects of turbulence intensity and integral length scale of a turbulent free stream on forced convection heat transfer from a circular cylinder in cross flow. In *Proceedings of the 6th International Heat Transfer Conference*, volume 5, pages 347–352.
- Zdravkovich, M. M. (1997). *Flow around circular cylinders*. Oxford University Press.

- Zhou, Y., Nagata, K., Sakai, Y., Ito, Y., and Hayase, T. (2016). Spatial evolution of the helical behavior and the 2/3 power-law in single-square-grid-generated turbulence. *Fluid Dyn. Res.*, 48:021404.
- Zhou, Y., Nagata, K., Sakai, Y., Suzuki, H., Ito, Y., Terashima, O., and Hayase, T. (2014). Relevance of turbulence behind the single square grid to turbulence generated by regular- and multiscale-grids. *Phys. Fluids*, 26:075105.
- Zukauskas, A. (1972). Heat transfer from tubes in crossflow. In Hartnett, J. P. and Irvine, T. F. J., editors, *Advances in Heat Transfer*. Academic Press.
- Zukauskas, A., Vaitiekunas, P., and Ziugzda, J. (1993). Analysis of influence of free stream turbulence intensity and integral length scale on skin friction and heat transfer of a circular cylinder. In *Experimental Heat Transfer, Fluid Mechanics and Thermodynamics 1993*, pages 591 – 596. Elsevier, Amsterdam.